applied sciences

MDPI

Article

Using Temperature-Programmed Photoelectron Emission (TPPE) to Analyze Electron Transfer on Metallic Copper and Its Relation to the Essential Role of the Surface Hydroxyl Radical

Yoshihiro Momose

Department of Materials Science, Ibaraki University, Hitachi 316-8511, Japan; y.momose@cpost.plala.or.jp

Abstract: Surface processes such as coatings, corrosion, photocatalysis, and tribology are greatly diversified by acid–base interactions at the surface overlayer. This study focuses on the action of a metallic copper surface as an electron donor/acceptor related to the inactivation of viruses. It was found that regarding Cu_2O or Cu materials, electrostatic interaction plays a major role in virus inactivation. We applied the TPPE method to clarify the mechanism of electron transfer (*ET*) occurring at light-irradiated copper surfaces. The TPPE characteristics were strongly influenced by the environments, which correspond to the temperature and environment dependence of the total count of emitted electrons in the incident light wavelength scan (PE total count, N_T), the photothreshold, and further the activation energy (ΔE) analyzed from the Arrhenius plot of N_T values obtained in the temperature increase and subsequent temperature decrease processes. In this study, we re-examined the dependence of the TPPE data from two types of Cu metal surfaces: sample A, which was mechanically abraded in alcohols, water, and air, and sample C, which was only ultrasonically cleaned in these liquids. The N_T for both samples slowly increased with increasing temperature, reached a maximum (N_{Tmax}) at 250 °C (maximum temperature, T_{max}), and after that, decreased. For sample A, the N_{Tmax} value decreased in the order H_2O > CH_3OH > C_2H_5OH > $(CH_3)_2CHOH$ > C_3H_7OH, although the last alcohol gave T_{max} = 100 °C, while with sample C, the N_{Tmax} value decreased in the order C_3H_7OH > $(CH_3)_2CHOH$ > C_2H_5OH > CH_3OH > H_2O. Interestingly, both orders of the liquids were completely opposite; this means that a Cu surface can possess a two-way character. The N_T intensity was found to be strongly associated with the change from the hydroxyl group (–Cu–OH) to the oxide oxygen (O^{2-}) in the O1s spectra in the XPS measurement. The difference between the above orders was explained by the acid–base interaction mode of the –Cu–OH group with the adsorbed molecule on the surfaces. The H_2O adsorbed on sample A produces the electric dipole $–CuO^{\delta-}H^{\delta+} \cdots :OH_2$ (⋯ hydrogen bond), while the C_3H_7OH and $(CH_3)_2CHOH$ adsorbed on sample C produce $RO^{-\delta}H^{\delta+} \cdots :O(H)–Cu–$ (R = alkyl groups). Gutmann's acceptor number (*AN*) representing the basicity of the liquid molecules was found to be related to the TPPE characteristics: $(CH_3)_2CHOH$ (33.5), C_2H_5OH (37.1), CH_3OH (41.3), and H_2O (54.8) (the *AN* of C_3H_7OH could not be confirmed). With sample A, the values of N_{Tmax}a and ΔEa_{Up1} both increased with increasing *AN* (Up1 means the first temperature increase process). On the other hand, with sample C, the values of N_{Tmax}c and ΔEc_{Up1} both decreased with increasing *AN*. These findings suggest that sample A acts as an acid, while sample C functions as a base. However, in the case of both types of samples, A and C, the N_{Tmax} values were found to increase with increasing ΔE_{Up1}. It was explained that the ΔE_{Up1} values, depending on the liquids, originate from the difference in the energy level of the hydroxyl group radical at the surface denoted. This is able to attract electrons in the neighborhood of the Fermi level of the base metal through tunnelling. After that, Auger emission electrons are released, contributing to the *ET* in the overlayer. These electrons are considered to have a strong ability of reducibility.

Keywords: TPPE; copper surface; electron transfer; photoelectron emission; abrasion; ultrasonic cleaning; temperature scan; wavelength scan; alcohols and water; acid and base interaction; activation energy; acceptor number; hydroxyl radical; reducibility; tunnelling; Auger emission

check for updates

Citation: Momose, Y. Using Temperature-Programmed Photoelectron Emission (TPPE) to Analyze Electron Transfer on Metallic Copper and Its Relation to the Essential Role of the Surface Hydroxyl Radical. *Appl. Sci.* **2024**, *14*, 962. https://doi.org/10.3390/app14030962

Academic Editors: Francis Verpoort and Abdeltif Amrane

Received: 1 December 2023
Revised: 29 December 2023
Accepted: 10 January 2024
Published: 23 January 2024

Copyright: © 2024 by the author. Licensee MDPI, Basel, Switzerland. This article is an open access article distributed under the terms and conditions of the Creative Commons Attribution (CC BY) license (https://creativecommons.org/licenses/by/4.0/).

1. Introduction

Improving the properties of surfaces and interfaces of practical products plays an important role in many surface phenomena, such as adhesion, heterogeneous catalysis, corrosion, triboelectric charging, contact electric potential, corrosion, and friction. Exoemission, a general name for many types of electron emission phenomena, can be observed from processed solid surfaces that one mechanically deforms or exposes to ionizing radiation and further covers with foreign materials such as an oxide layer. Such electron emission is because of a surface-dependent effect rather than clean surfaces. Recently, the author has published a book titled *exoemission from processed solid surfaces and gas adsorption* [1]. In the book, temperature-programmed photoelectron emission (TPPE) is outlined. This method is a useful measurement for distinguishing differences in the electronic properties of base metals and further in the electron transfer in the surface overlayer.

TPPE has the ability to provide useful information on the properties of electron transfer in the neighborhood of the surface of the solids and is completely different from methods such as X-ray photoelectron spectroscopy (XPS), which is described later, and temperature-programmed reaction (TPR).

Morrison [2] described that for antimicrobial effects, copper's specific atomic makeup gives it extra killing power. Excellent reviews on the function of metallic materials to deactivate viruses and bacteria have been reported [3–6]. In Ref. [3], the effects of the chemical nature of metals and metal-based materials on the inactivation of viruses have been reviewed widely and summarized: (1) antiviral performances of different metallic materials such as copper nanoparticles; (2) antiviral mechanisms at the biological level such as the blockade of virus spread and infection in porous metallic materials or metallic materials with positive charges on the surface; direct inactivation of the virus such as the contact of metallic materials with the virus and the reaction of metallic materials with oxidants and reductants in the environment to generate reactive oxygen species (e.g., hydroxyl radicals and superoxide anions), which can effectively damage the proteins and genetic material of viruses; (3) potential antiviral mechanisms at the physicochemical level. However, it was said that researchers in different fields hold dissimilar views on the antiviral mechanisms; the authors hope that this review helps researchers in various fields to select suitable substrates for antiviral materials based on the chemical nature of metal elements. Further, emphasis is placed on the fact that the strong reducibility of metal nanoparticles may be the main reason for their efficient inactivation of viruses. This remark has prompted our attention to study how the chemical nature of reducibility on metallic copper may be related to the behavior of *ET* on copper metal surfaces with adsorption layers of alcohols, water, and air. In the reviews [4,5], it is described that there are two substances that can destroy viral proteins: hydroxyl radicals and superoxide ions, which are generated by Cu released from CuI in water. Reactive hydroxyl radicals can be generated in a Fenton-type reaction. It is well known that corrosion requires both a continuous ionic path and electrical connection between the anode and cathode in the same location. The review [6] outlines that in atmospheric corrosion of a copper surface oxidized in air, which corresponds to the environment of the sample surfaces used in the present experiment, there is a thin film of aqueous solution which enables corrosion processes to proceed. The typical cathodic reaction during copper corrosion is the oxygen reduction reaction. The mechanism produces hydrogen peroxide (H_2O_2) as an intermediate. This may result in a metal ion and hydrogen peroxide at the same or nearby sites. We are interested in the following studies related to the inactivation of viruses by Cu_2O: (1) The high antibacterial efficacy of Cu_2O suggests that oxide formation on copper objects in a dry atmosphere does not impair their efficiency as an antimicrobial measure. The influences of bacteria–metal interaction, media composition, and copper surface chemistry on contact killing are not fully understood [7–9]. (2) Cu_2O has a unique antiviral mechanism mediated by direct contact [10,11]. (3) The preparation of small-sized nano Cu_2O particles on halloysite nanotubes has been carried out. Most importantly, HNTs with positive charges on the surface could enhance their interaction with bacteria and cause physical damage [12,13].

(4) The specimens, which existed as mainly Cu^0 or Cu^+ on the surface, exhibit the same corrosion behavior and promote the elution of Cu ions due to the presence of *E. coli* in the immersion solution. In contrast, the release of Cu ions from the specimen that existed mainly as Cu^{2+} does not change in the presence of bacteria [14–17]. (5) Photo-electro-Fenton reaction and surface hydroxyl groups [18–22] and biocorrosion stability and biosynthesis of metal oxide nanoparticles [23,24] are of great importance.

Further, from the cathodic reduction of copper oxides (CuO and Cu_2O) in a strongly alkaline electrolyte [25], it is assumed that there is a limiting thickness of the Cu_2O layer. This results from competition of the disproportionation reaction ($Cu + CuO \rightarrow Cu_2O$) and CuO formation ($Cu_2O + (1/2)O_2 \rightarrow 2CuO$), and it is suggested that $Cu(OH)_2$ plays an initial key role in the growth of the corrosion layer.

Surface processes are further diversified by acid–base interactions at the surface overlayer. Acid–base reactions between adsorbates and metal oxides or hydroxides/metals are strongly influenced by electron donors/acceptors governing the *ET* behavior at the surface overlayer. We developed an extremely sensitive surface analysis technique of *ET* using photoelectron emission (PE), which is measured as a function of temperature. This method is called temperature-programmed photoelectron emission (TPPE). We have reported several papers on TPPE [26–28]. The TPPE feature for the surfaces of 17 commercial metals was correlated with their surface chemical structure measured by XPS [27,28]. The metals used were distinctly classified into two main groups (A and B): the former indicated a temperature-dependent PE total count, while the latter indicated a virtually temperature-independent PE total count. The A group included Al, Pt, Pb, Cu, Ag, Au, and Ni; the B group included Ta, Ti, Mo, Pd, W, Fe, Co, Zn, Nb, and Sn [27,28]. Further, we found that when a copper electrode was used in the electrochemical reduction of carbon dioxide, the copper surface exhibiting an increased PE total count tended to produce a greater amount of CH_4 as the reduction product [29].

The purpose of the present study is to clarify the TPPE characteristics of metallic copper samples mechanically abraded in alcohols, water, and air and ultrasonically cleaned in the liquids, and further, its relation to the properties of the liquids. We have already reported that two types of copper surfaces showed completely different TPPE behavior, but although it is of great interest, the reason why it occurs was not fully understood [26]. In this study, in view of the importance of the surface treatment of metallic copper, we tried to account for the mechanism of TPPE based on the acid–base interaction.

First, we describe the important points of the TPPE method and briefly feature the present understanding of the TPPE results. Regarding the species and interaction modes appearing in the TPPE method are as follows: (a) The key functional group: –OH group adsorbed on the metal surface and its polarity; (b) the electron density of the oxygen of –OH group, which depends on the negative electric potential and the intensity of irradiated light; (c) the orientation of adsorbate molecules due to the acid–base interaction in the adsorption on the –OH group; (d) the formation of electric dipoles between the –OH group and adsorbate molecules; (e) the change in the components of O1s spectra before and after the TPPE measurement.

The dependence of TPPE on temperature and environment is quantified using PE stimulation spectra [26]. The following data and its relationship to the properties of the adsorbate molecules are obtained: (a) the total count of emitted electrons in the incident light wavelength scan (PE total count, N_T), which may correspond to the transport distance of electrons released from the base metal. (b) The photothreshold representing the minimum photon energies needed to remove an electron from the surface of a material. But in this study, the values were not estimated. (c) The activation energies of N_T for all Cu samples were obtained from an Arrhenius-type equation of $N_T = A_{0NT} \exp(-\Delta E/kT)$, where A_{0NT} indicates the pre-exponential factor, k is the Boltzmann factor, and T is Kelvin. This expression was applied to N_T values in the temperature increase and subsequent temperature decrease processes. (d) The relation of activation energies of ΔE_{Up1} (Up1 indicates the first temperature increase process) to Gutmann's acceptor number (AN), representing

basicity, and the reciprocal of dielectric constant ($\varepsilon/\varepsilon_0$) of the used liquids is examined. Regarding contact killing of viruses by metals, the action of electrons accumulated in the neighborhood of the reaction site is considered to be most essential according to Ref. [3], because of the increase in the reducibility of the metal. As the electron emission mechanism will be described in detail later, electrons in the base metal are captured by hydroxyl group radicals adsorbed at the surface, and then, Auger emission occurs, giving rise to a PE stimulation spectrum. ΔE is considered to correspond to the trap depth of the hydroxyl group radical to attract electrons from the base metal. Further, we are interested in the relation of AN to $1/(\varepsilon/\varepsilon_0)$ of the liquids. As shown later it was found that the $1/(\varepsilon/\varepsilon_0)$ decreases with increasing AN for the liquids. The dependence of ΔE on $1/(\varepsilon/\varepsilon_0)$ is also clarified for the liquids.

The relation of TPPE to the XPS results is featured as follows: (a) Two components of O1s spectra, –OH (hydroxyl group) and O^{2-} (oxide), are of great importance. (b) The increase in N_T in PE stimulation spectra is confirmed to be strongly related to the increase in the intensity of –OH before the TPPE measurement. After the TPPE measurement, only the O^{2-} component appears and the N_T disappears. Although the detailed mechanism of the –OH group adsorbed at the surface is not clear, it is considered that it has the character of a radical, with the ability to attract electrons by tunnelling from the base metal, followed by Auger emission. The PE stimulation spectra appear as a result of the Auger emission. The ability of the hydroxyl group radical to attract electrons is influenced by the acid–base interaction between the –OH group and the liquids adsorbed around the –OH group, producing different ΔEs.

2. Materials and Methods

2.1. Materials

Rolled copper sheets (Nilaco Corporation, Tokyo, Japan, thickness 0.1 mm, purity 99.9%) were used. The size of metal samples was 30 × 20 mm^2 (for TPPE) and 3 × 3 mm^2 (for XPS). Prior to use, these sheets were pretreated by successive ultrasonic cleaning in n-hexane (5 min), distilled water (5 min), acetone (5 min), and distilled water (5 min). The volume of each liquid used was 50 mL, respectively. Finally, the samples were dried in a vacuum for 10 min. Before the TPPE measurement, a pretreated metal sheet was subjected to abrasion or ultrasonic cleaning in liquids of methanol , Yamato(CH_3OH), ethanol (C_2H_5OH), 1-propanol/(C_3H_7OH), 2-propanol (($CH_3)_2CHOH$) (all reagent grade), and distilled water, and also to abrasion in ambient air. The treatment of metal sheets was conducted as follows: First a metal sheet was immersed in 50 mL of each liquid described/above or exposed to ambient air in a glass beaker, and then was abraded by rotating an iron screw on the sheet surface at a rate of 300 rpm using an external magnetic stirrer at room temperature. The/abrasion periods were 5, 10, and 30 min. The ultrasonic cleaning alone in the liquids was also performed for 5 min using an ultrasonic cleaner (Branson 1210J, Yamato Scientific, Tokyo, Japan). After that, the metal sheets were dried in a vacuum for 10 min.

2.2. TPPE and XPS

Figure 1 shows the arrangement of the TPPE measurement apparatus which was used in the present study and in Ref. [26]. It consists of the following parts: a UV light source (Hamamatsu Photonics, D_2 lamp, L613, Hamamatsu, Japan), a monochromator, an electron counter with anode, the voltage of which was set at 1400 V, and a sample holder with a Nichrome wire heater. A −94 V negative potential relative to the grounded grid (denoted by a dotted line in Figure 1) was applied to the holder using a battery to accelerate and collect emitted electrons. The negative potential applied to the sample holder should be observed to act in the same way as the cathodic reduction in corrosion. The counter gas was Q gas (He and ~1% isobutane (iso-C_4H_{10})) and its flow rate was ~100 bubbles min^{-1}. The PE intensity (indicated by the unit of count min^{-1}) was measured by varying the wavelength of the light from 300 to 170 nm at a rate of 20 nm min^{-1}. A spot of 0.5 × 5 mm^2 on the

sample was illuminated by the light. We call the curve of the PE intensity vs. wavelength a PE stimulation spectrum. For one sample, the PE spectra were measured 12 times at different temperatures in the temperature increase and subsequent temperature decrease processes between 25 and 350 °C (usually the data for the temperature increase process were employed). The measurement temperature was successively changed at the interval of 50 °C.

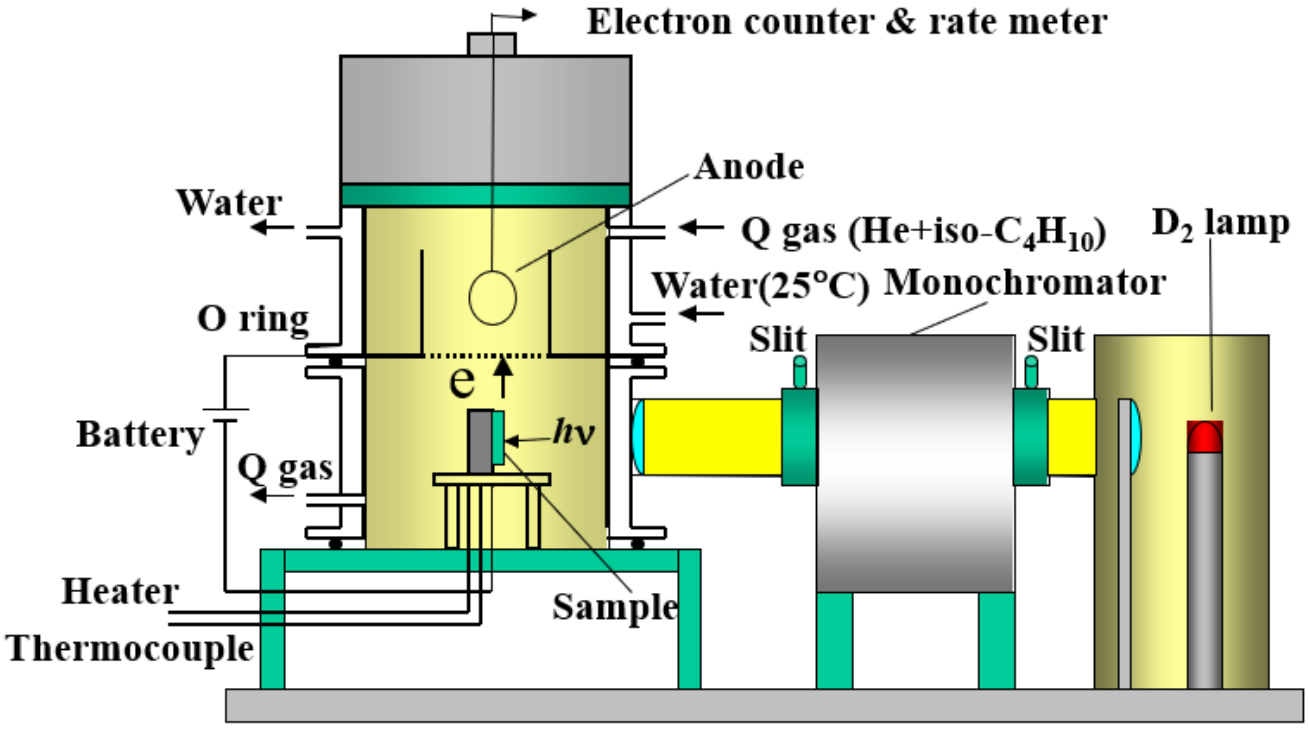

Figure 1. The temperature-programmed photoelectron emission (TPPE) measurement apparatus (The arrows written in the figure indicate the inlet and outlet of Q gas and constant temperature water, and the direction of irradiation of photons ($h\nu$) and collection of emitted electrons).

The XPS spectra of Cu2p, Cu_{LMM}, O1s, and C1s before and after the TPPE measurement were measured on a Shimadzu ESCA 750 spectrometer (Kyoto, Japan) with an X-ray source of Mg Kα (8 kV and 30 mA) and processed with an ESCAPAC 760 analyzer (Kyoto, Japan). It should be noted that before and after the TPPE measurement, the samples were once exposed to ambient air to move the samples to the XPS spectrometer. The start–stop energy and the response factor for the XPS spectra used to obtain the elemental composition were as follows: Cu2p (965–925 eV, 24.1), Ols (540–528 eV, 2.9), C1s (295–280 eV, 1.0), Cu_{LMM} (350–325 eV), and Cu3p (82–70 eV). The binding energy of these spectra was corrected by assigning the main carbon component to the binding energy of 285 eV.

3. Results and Discussion

3.1. PE Stimulation Spectra and TPPE Plot

Figure 2 shows typical PE stimulation spectra observed during wavelength scans in the temperature increase process for copper samples abraded in CH_3OH [26] and abraded and cleaned only in C_2H_5OH. The intensity of PE increases progressively and reaches a maximum, followed by a decrease with decreasing wavelength of the light (or increasing photon energy). An emission peak appears around 220–200 nm. In Figure 2(1), the PE intensity of the peak in the PE stimulation spectrum decreases and interestingly shifts to a shorter wavelength with increasing abrasion time. In Figure 2(2), the emission peak of all the spectra yields the maximum at 250 °C. We call the total number of emitted electrons in the PE stimulation spectra PE total count (N_T).

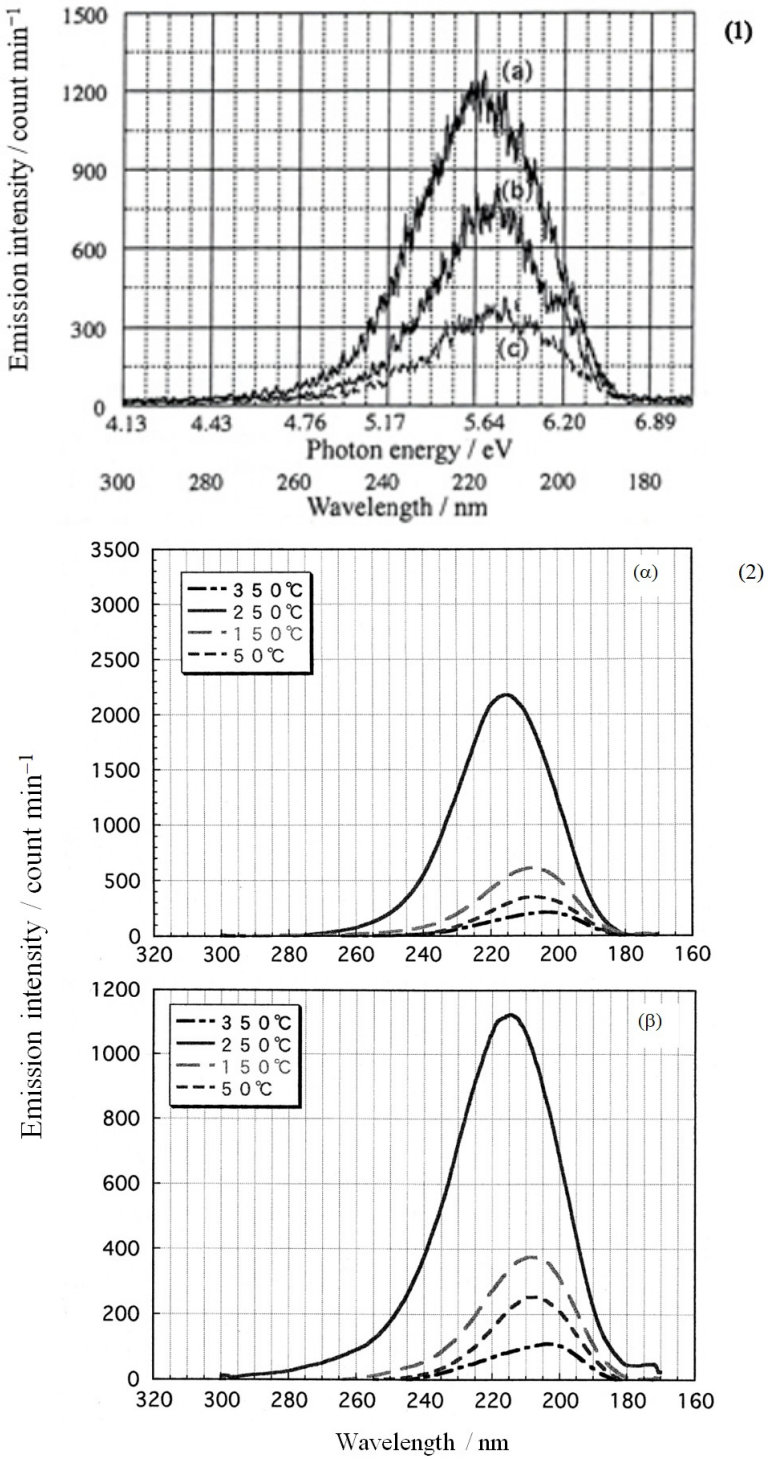

Figure 2. Examples of typical PE stimulation spectra in the temperature increase process: (**1**) Effect of abrasion time on PE measurement at 250 °C for copper samples abraded in CH_3OH. Abrasion time: (a) 5 min, (b) 10 min, and (c) 30 min. (**2**) Effect of ultrasonic cleaning only and abrasion in C_2H_5OH on PE measurement for copper samples: (α) cleaning for 5 min and (β) abrasion for 10 min.

Figure 3 shows the TPPE plots of N_T vs. temperature during the 1st and 2nd temperature increase and subsequent temperature decrease processes for copper samples (sample A) abraded for 10 min in various environments: (1) H_2O, (2) CH_3OH, (3) C_2H_5OH, (4) $(CH_3)_2CHOH$, (5) C_3H_7OH, and (6) ambient air. This plot is called the TPPE plot. It should be noted that in the TPPE plot, the corrected values of N_T were used by deducting

the natural count (1000 counts). The TPPE plot in the Up1 process exhibits a markedly different behavior from that in other processes; that is, in each environment, the value of N_T remains low at the initial stage, starts to increase at 100 °C, and reaches a maximum at 250 °C, followed by a decrease, except for the TPPE plot for C_3H_7OH, which gives the maximum at 100 °C, being completely different from the other environments. Therefore, we have paid much attention to the TPPE plot in the Up1 process. For the abraded Cu samples, the effect of the abrasion periods (5, 10, and 30 min) on the TPPE characteristics is featured as follows [26]. In the cases of H_2O, CH_3OH, and C_2H_5OH, there is little difference in the N_T values at low temperature, but the growth of N_T values with increasing temperature is suppressed with an increase in the abrasion period, producing the most pronounced difference at 250–300 °C. The values of N_T become very small at 350 °C. A striking observation in these cases is that the N_T value yields a distinct maximum at 250–300 °C. This maximum tends to appear at a higher temperature, and clearly, the level of the maximum N_T for CH_3OH and C_2H_5OH lowers with increasing abrasion periods, although in the case of H_2O, the maximum decreases in the order 10 min > 5 min > 30 min. In the case of the abraded samples, two small broad peaks appear around 100 °C and 250–300 °C for C_3H_7OH, and one peak appears at 300 °C for $(CH_3)_2CHOH$, resulting in a very small effect of the abrasion period on the TPPE plot. Concerning the state of the metal surfaces, it was found that the surface abraded in C_3H_7OH becomes apparently bare compared to that in CH_3OH. In the case of air, the TPPE plots of the abraded surfaces for the abrasion periods yields a similar shape, with a maximum around 50–300 °C. This result shows that the TPPE was nearly constant, independently of the abrasion period.

Figure 4 shows the TPPE plots of N_T vs. temperature during the 1st and 2nd temperature increase and subsequent temperature decrease processes for copper samples (sample C) ultrasonically cleaned for 5 min in various liquids: (1) H_2O, (2) CH_3OH, (3) C_2H_5OH, (4) $(CH_3)_2CHOH$, and (5) C_3H_7OH. In the cases of CH_3OH and C_2H_5OH, the N_T values for samples only ultrasonically cleaned were comparable with those for the 10 min abraded samples. In the case of H_2O, the N_T for the 10 min abrasion sample was greatly larger than that for the sample ultrasonically cleaned in the liquid. In the cases of C_3H_7OH and $(CH_3)_2CHOH$, interestingly, a great difference was observed in the levels of N_T values between the ultrasonically cleaned and abraded samples; that is, the TPPE plot for the ultrasonically cleaned sample exhibited a distinct maximum at 250 °C, while that for the abraded samples gave a decreased level in the entire temperature range.

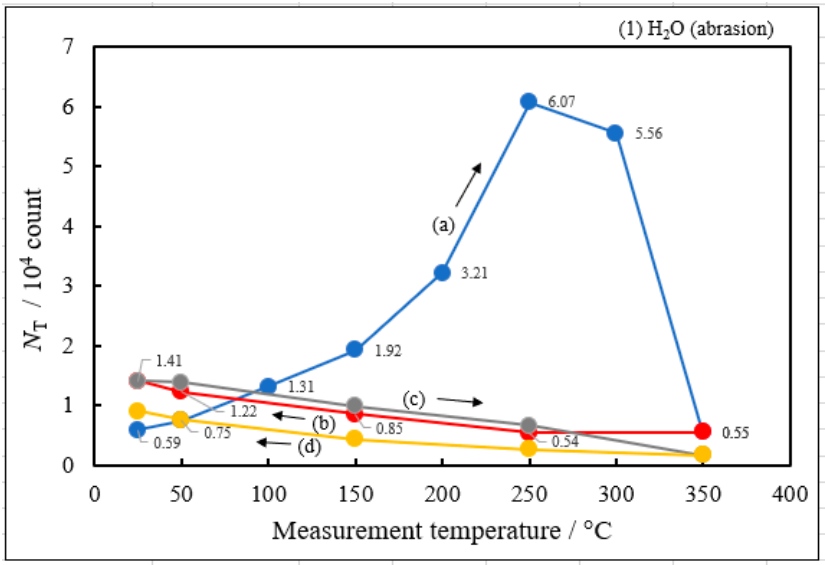

Figure 3. *Cont.*

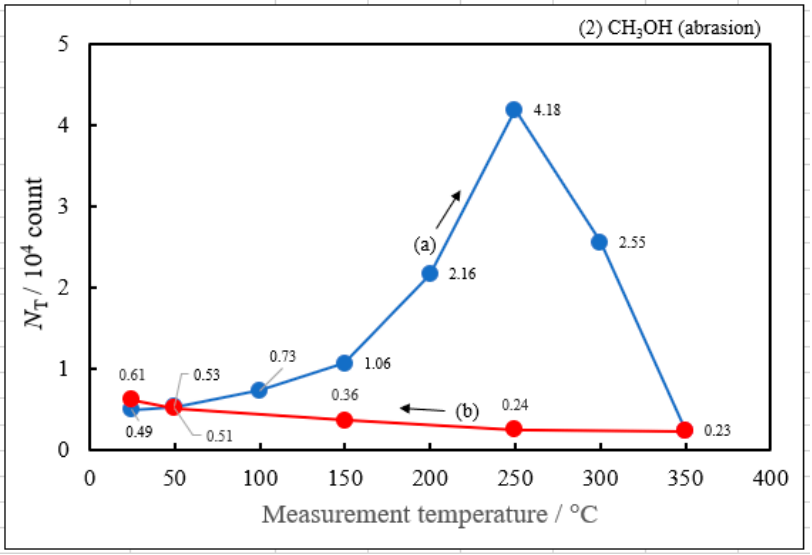

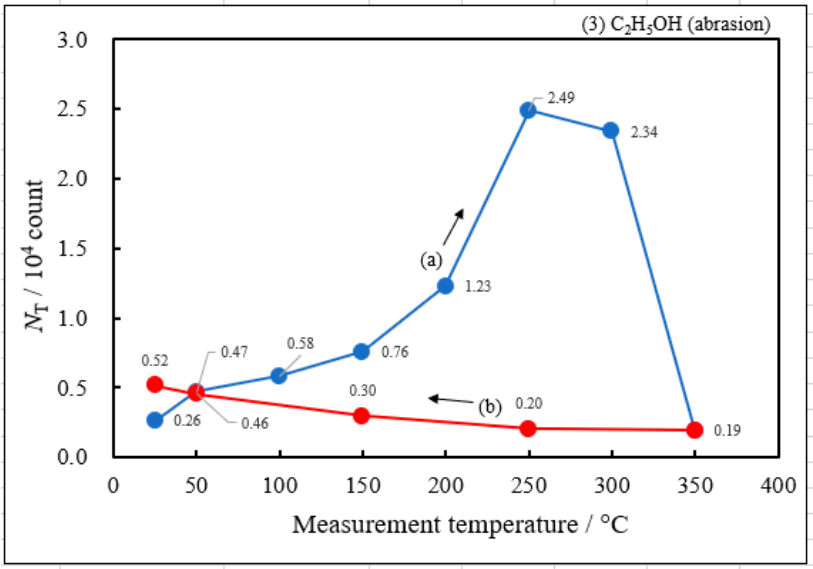

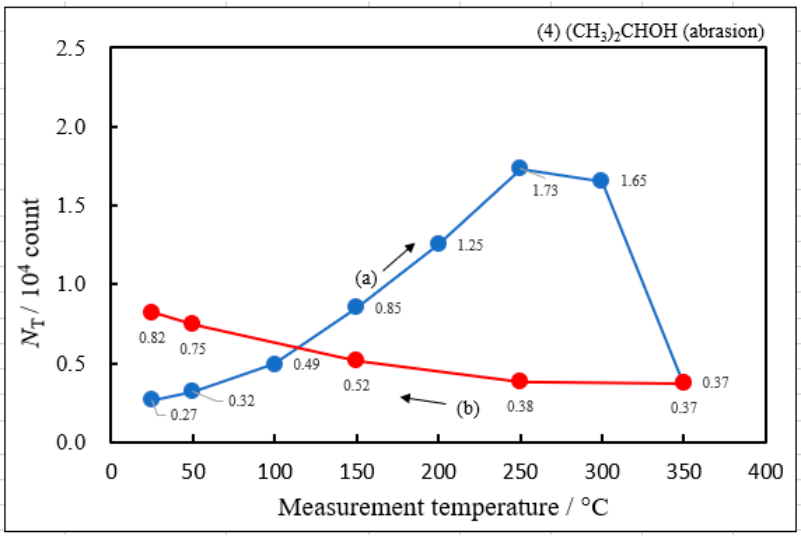

Figure 3. *Cont*.

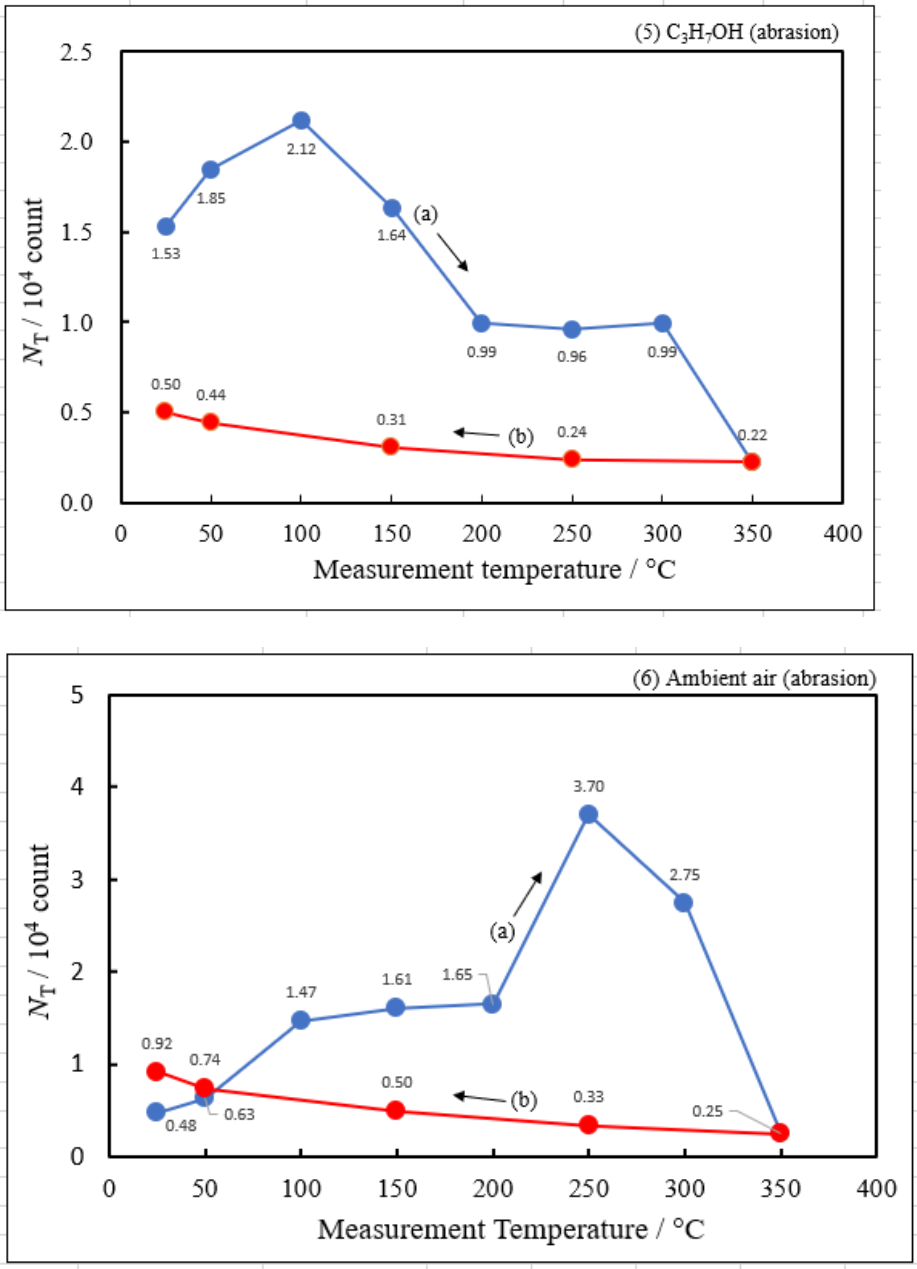

Figure 3. [Sample A] Plots of PE total count (N_T) during the 1st and 2nd temperature increase and subsequent temperature decrease processes for copper samples abraded in various liquids and in ambient air for 10 min, which are named (a) (Up1, blue line) and (b) (Down1, red line), and (c) (Up2, grey line) and (d) (Down2, yellow line), respectively, versus measurement temperature: (**1**) H_2O, (**2**) CH_3OH, (**3**) C_2H_5OH, (**4**) $(CH_3)_2CHOH$, (**5**) C_3H_7OH, and (**6**) ambient air. It is noted that the liquids are arranged in the decreasing order of the N_{Tmax}a.

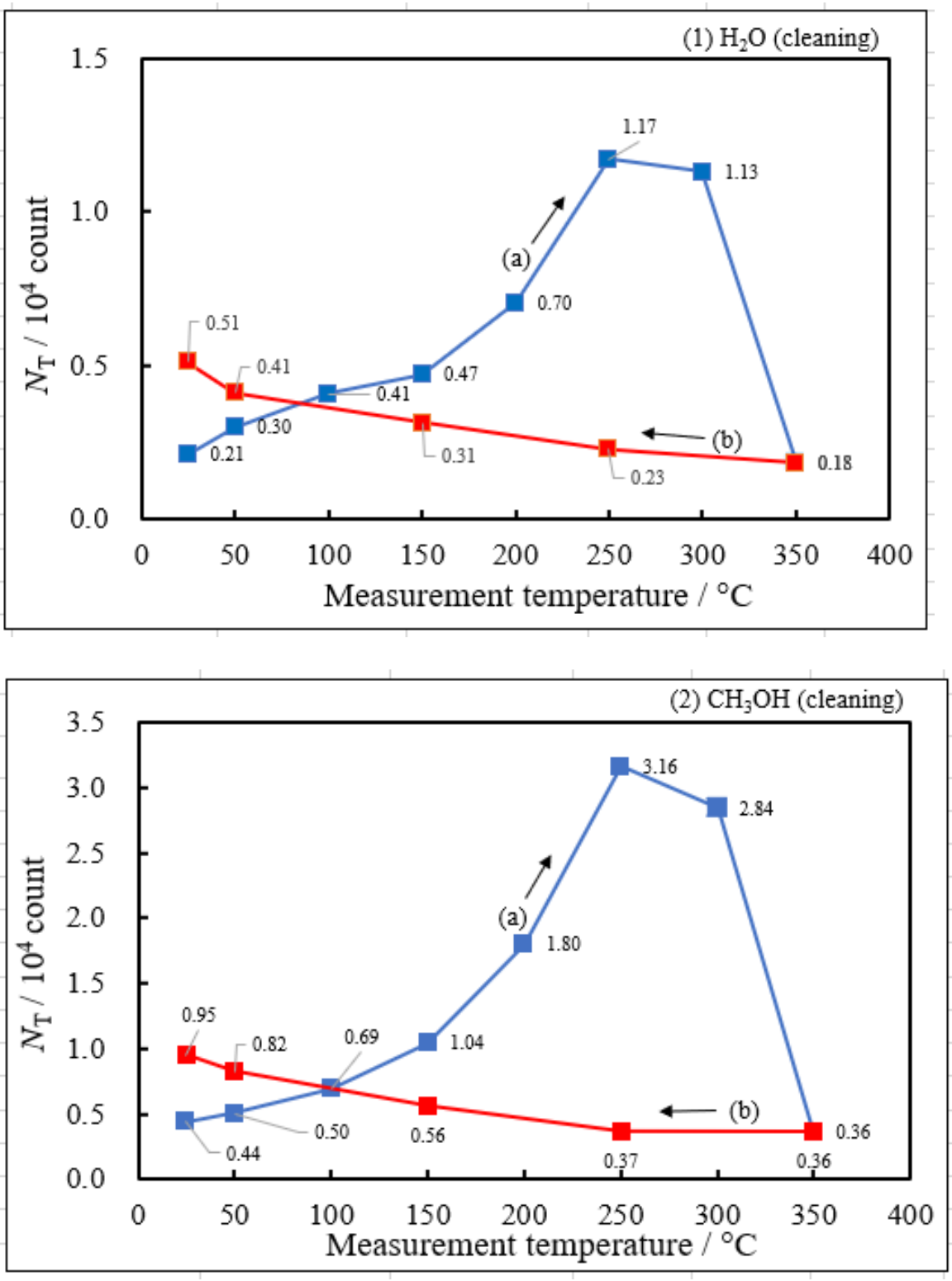

Figure 4. *Cont.*

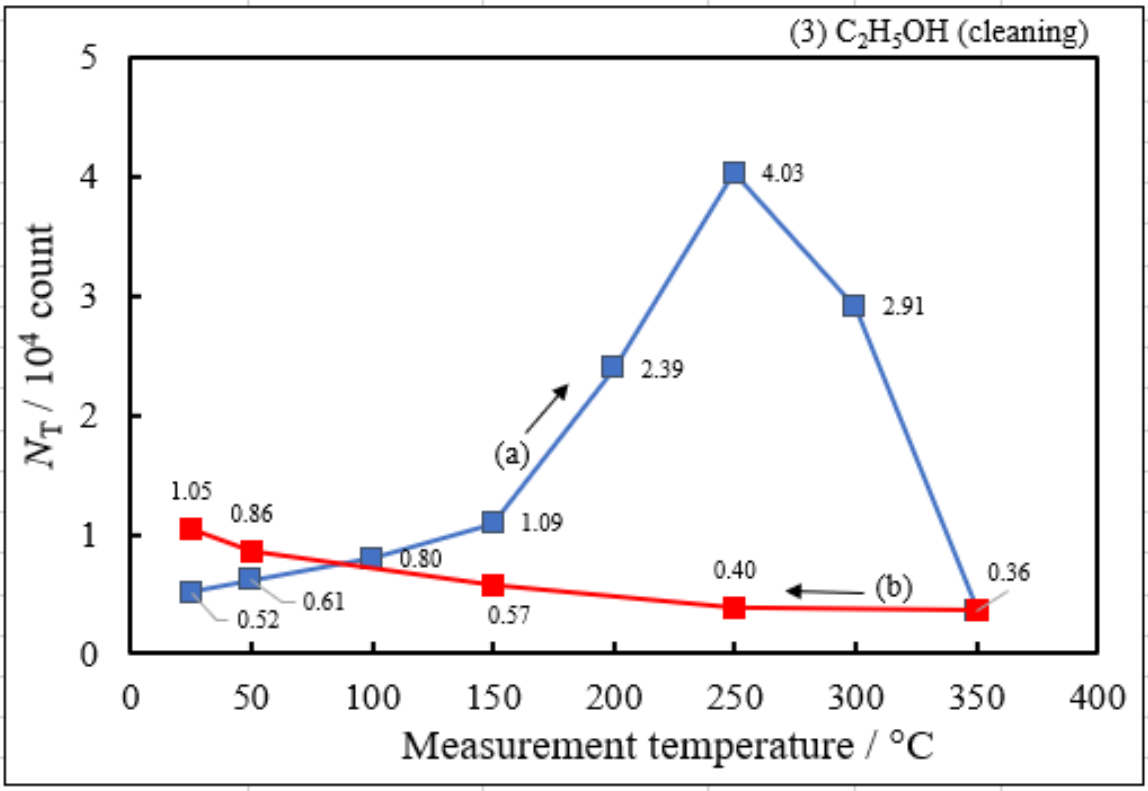

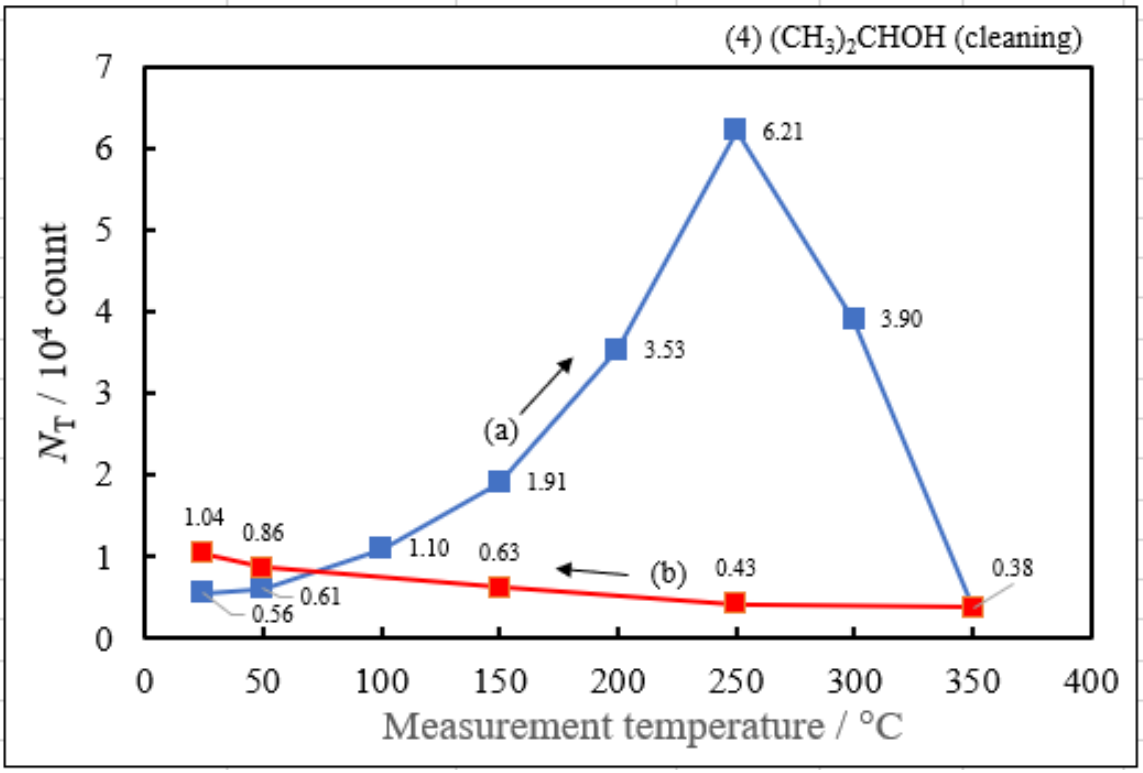

Figure 4. *Cont.*

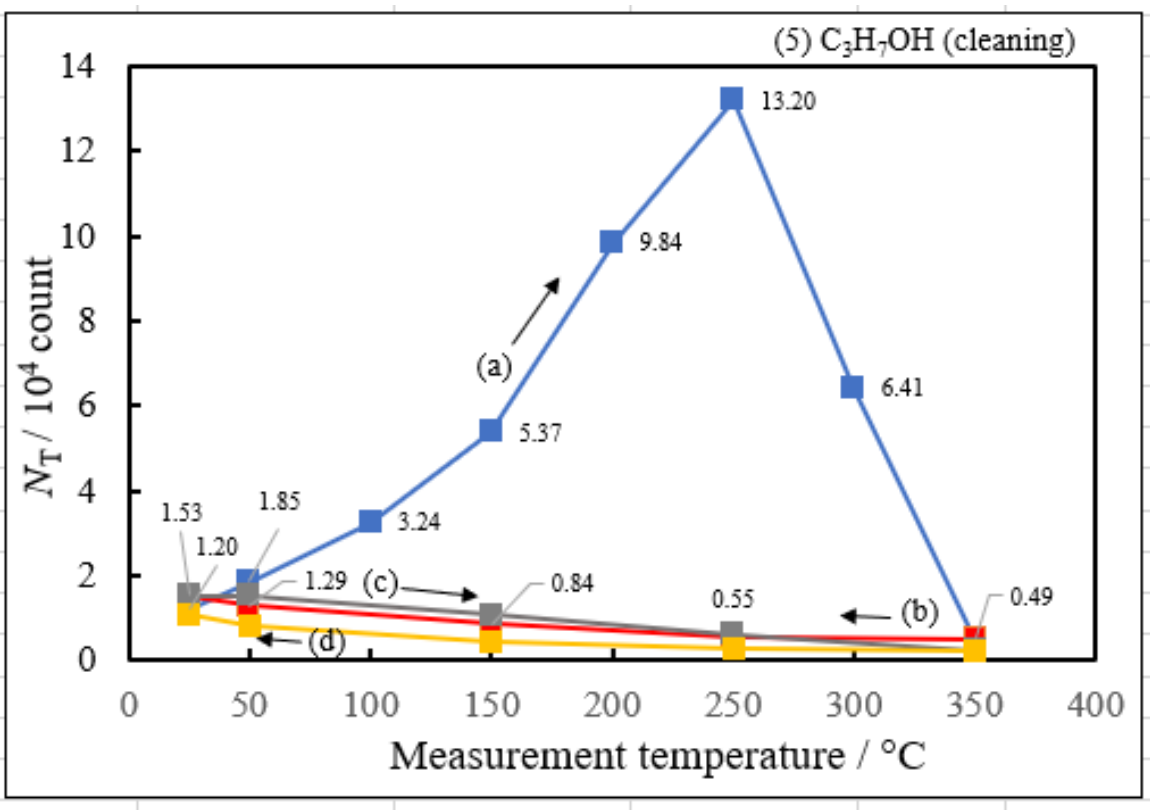

Figure 4. [Sample C] Plots of PE total count (N_T) during the 1st and 2nd temperature increase and subsequent temperature decrease processes for copper samples ultrasonically cleaned in various liquids for 5 min, which are named (a) (Up1 scan, blue line) and (b) (Down1 scan, red line), and (c) (Up2 scan, grey line) and (d) (Down2 scan, yellow line), respectively, versus measurement temperature: (**1**) H_2O, (**2**) CH_3OH, (**3**) C_2H_5OH, (**4**) $(CH_3)_2CHOH$, and (**5**) C_3H_7OH. It is noted that the liquids are arranged in the increasing order of the N_{Tmax}c.

Here, it should be noted that the TPPE plots in the processes other than Up1, that is, those in Down1, Up2 and Down2 scans, shown in Figures 3 and 4 will be referred to later. The Down1 scan was applied for all of the environments, and the Up2 and Down2 scans were applied for H_2O (Figure 3) and C_3H_7OH (Figure 4), which yielded the largest N_T value, in each case. It is confirmed that in these processes, the N_T values slowly increase with decreasing temperature and the levels of the N_T values are almost similar. We will describe the mechanism for PE occurring through Cu_2O.

3.2. Dependence of the TPPE Plots on Environments

Figure 5 shows the dependence of the TPPE plots for copper samples subjected to ultrasonic cleaning and 10-minute abrasion on the alcohols and water, including the data points for air [26]. In each sample, the TPPE plots exhibit a similar trend for the environments, except that for 10-minute abrasion in C_3H_7OH. The PE total count (N_T) slowly increases, reaches a maximum, and then decreases. In the case of 10-minute abrasion (sample A), the N_T value at 250 °C considerably decreased in the order H_2O > CH_3OH > C_2H_5OH > $(CH_3)_2CHOH$ > C_3H_7OH. On the other hand, in the case of ultrasonic cleaning (sample C), the N_T value decreased in the order C_3H_7OH > $(CH_3)_2CHOH$ > C_2H_5OH > CH_3OH > H_2O. The orders of N_T values for the two samples were completely opposite. This finding triggered the present study.

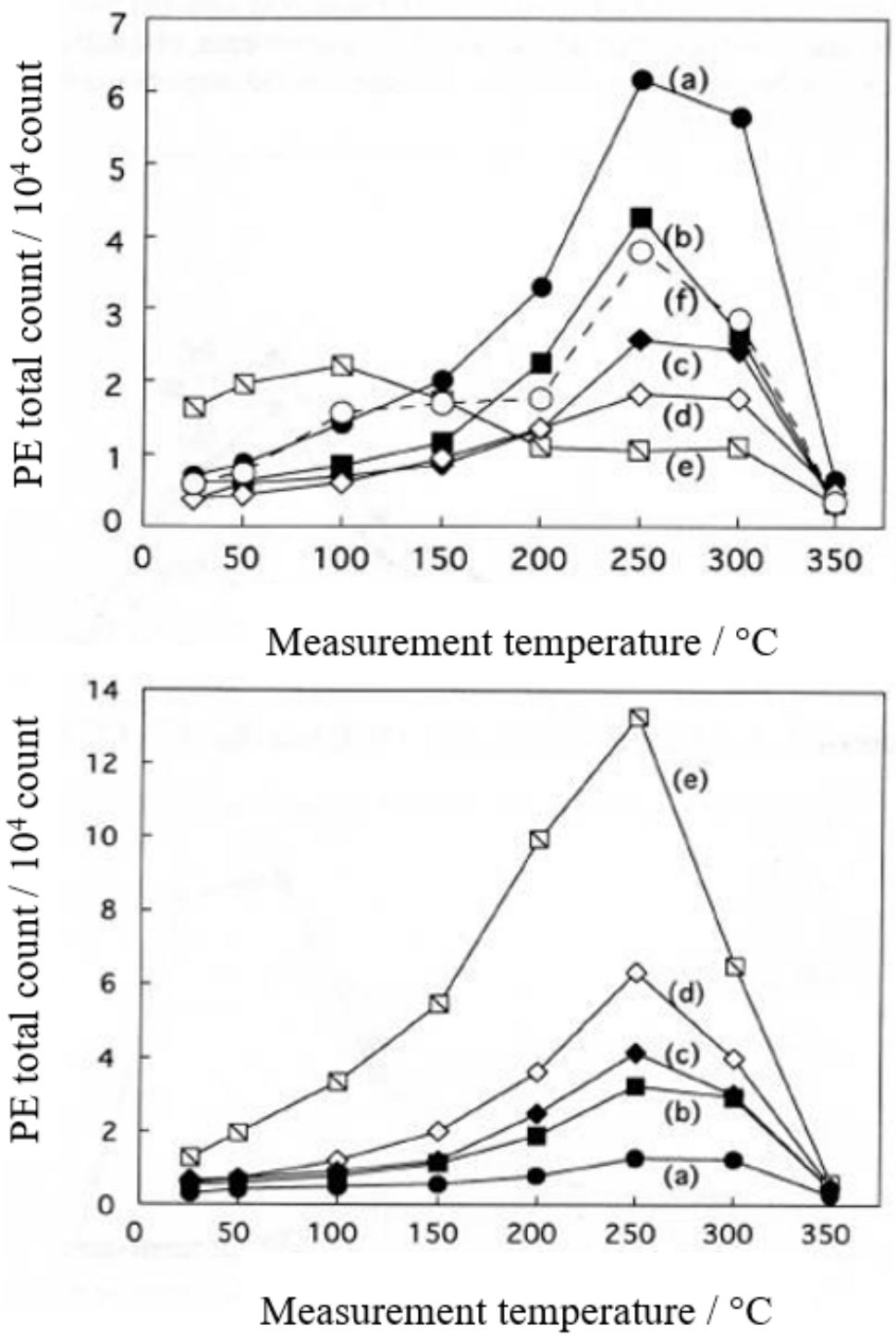

Figure 5. Dependence of N_T vs. temperature (TPPE plot) for copper samples subjected to 10-minute abrasion (sample A, **above**) and ultrasonic cleaning alone (sample C, **below**) on the liquids and air: (a) H_2O, (b) CH_3OH, (c) C_2H_5OH, (d) $(CH_3)_2CHOH$, (e) C_3H_7OH, and (f) ambient air.

3.3. XPS Spectra and XPS Characteristics

Figure 6 shows XPS spectra before and after the TPPE measurement for copper sheets subjected to only ultrasonic cleaning for 5 min in the liquids and mechanical abrasion for different periods of 5 min, 10 min, and 30 min in the liquids and ambient air: H_2O, CH_3OH, C_2H_5OH, $(CH_3)_2CHOH$, C_3H_7OH, and ambient air. We paid attention to three points, Cu_{LMM}, O1s, and the shake-up satellite structure 6–10 eV above the main Cu2p peak.

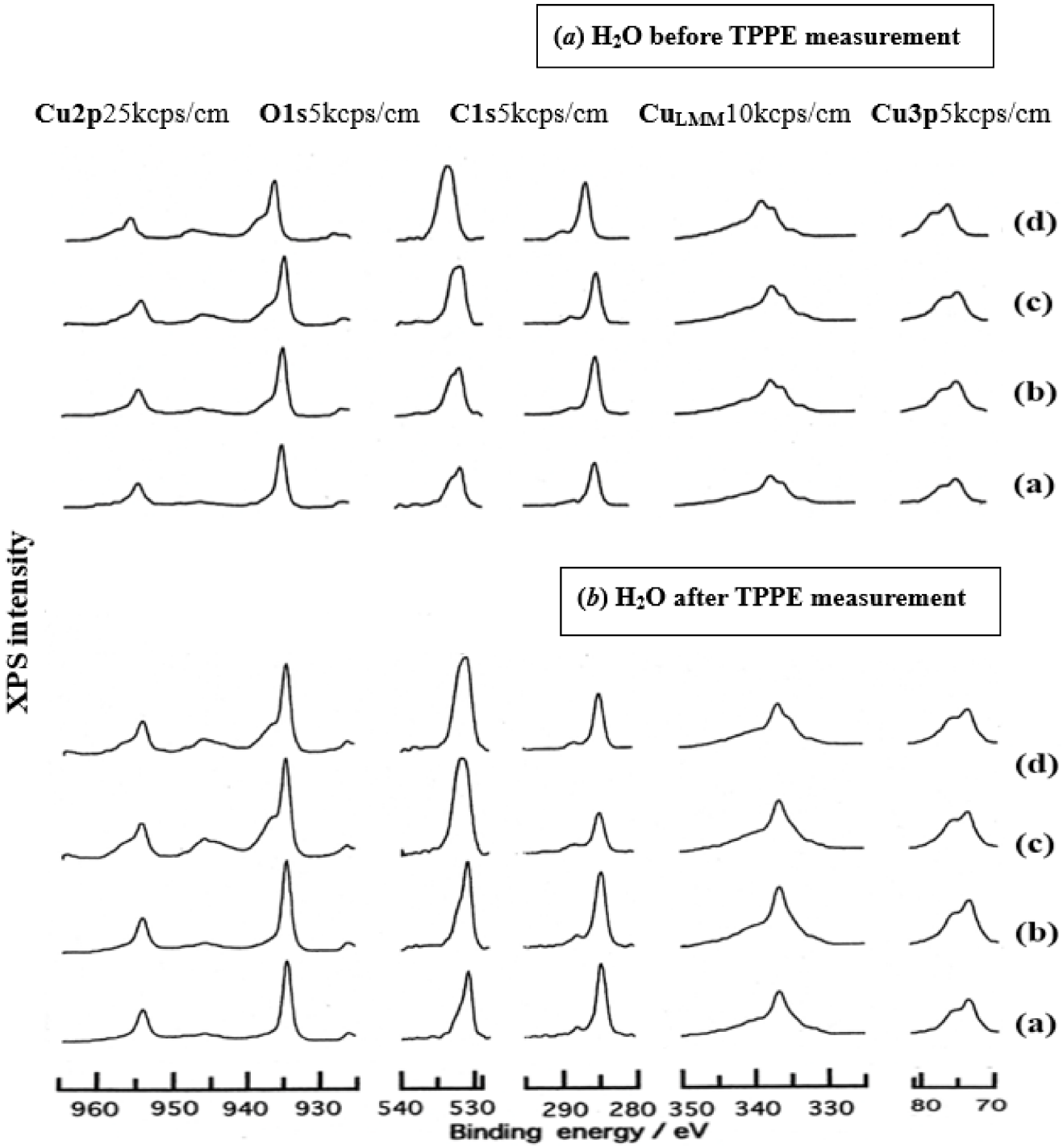

Figure 6. *Cont*.

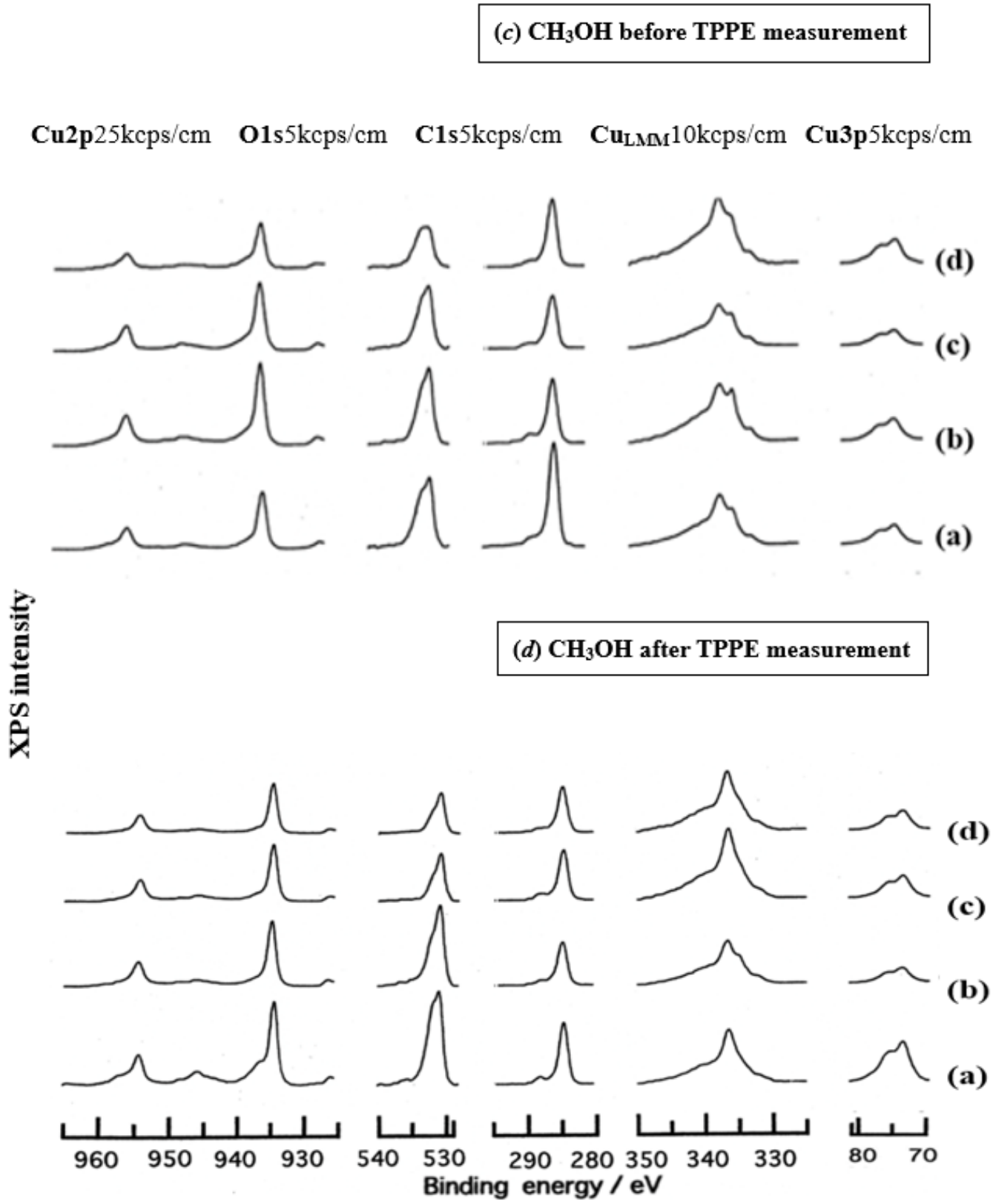

Figure 6. *Cont*.

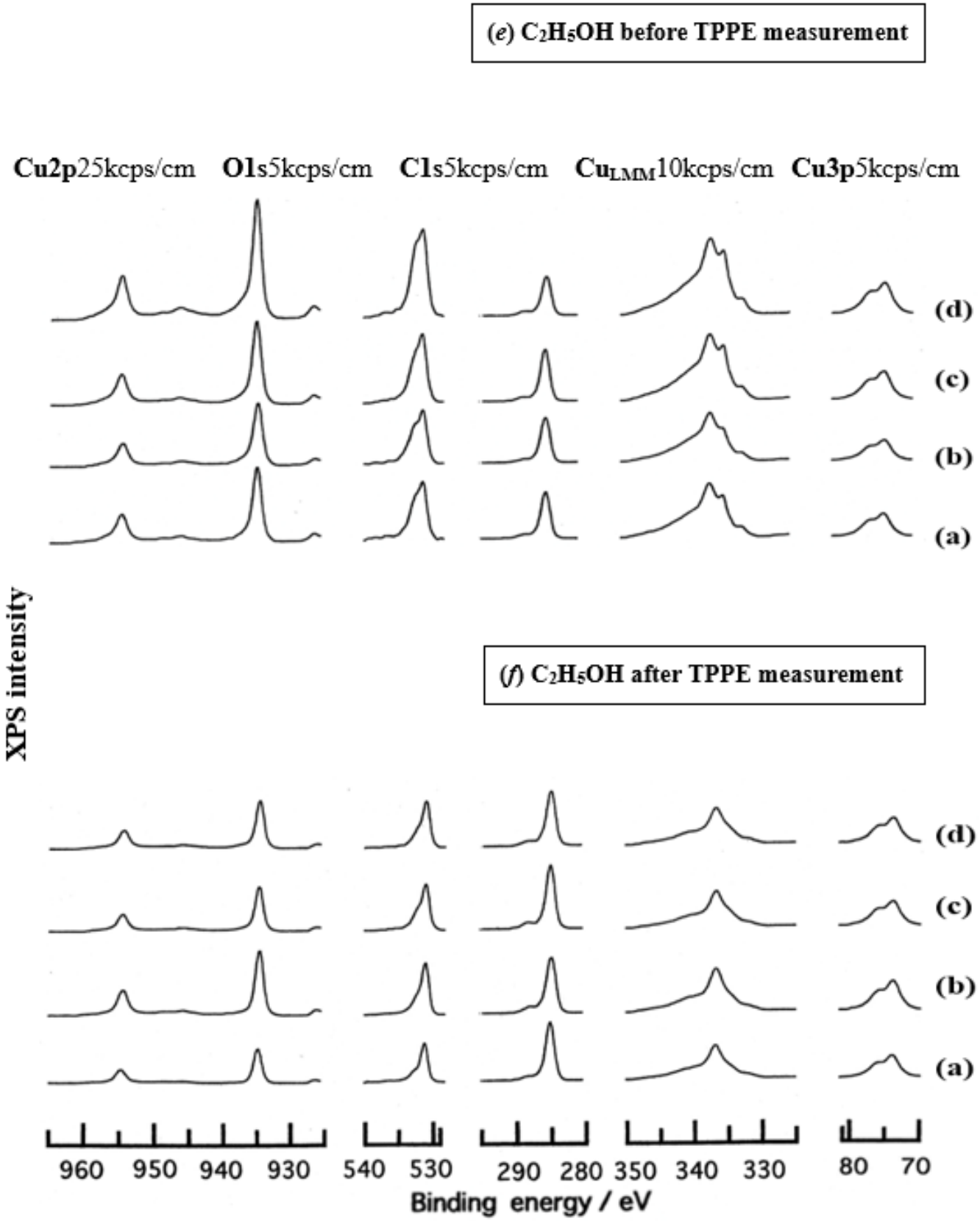

Figure 6. *Cont*.

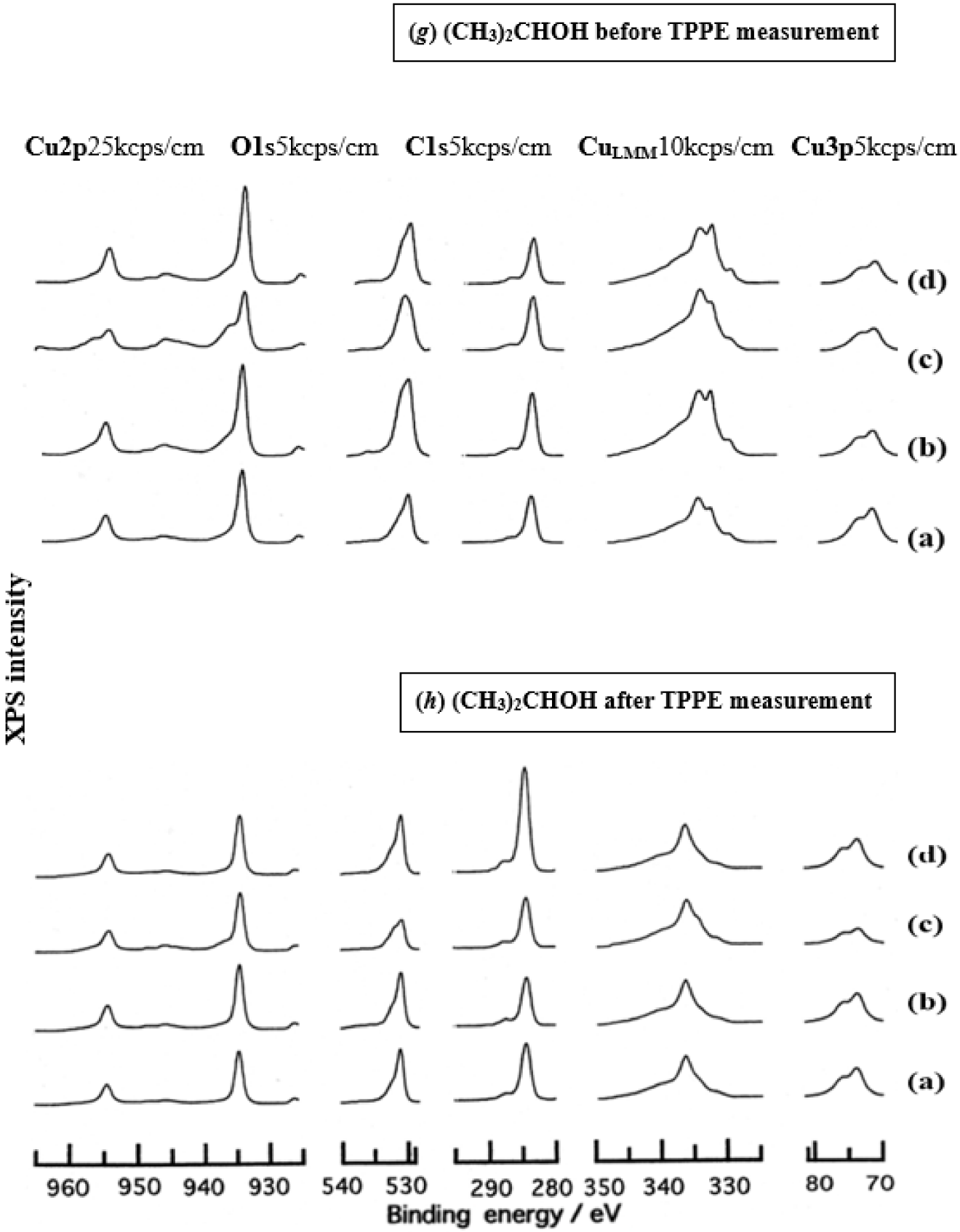

Figure 6. *Cont*.

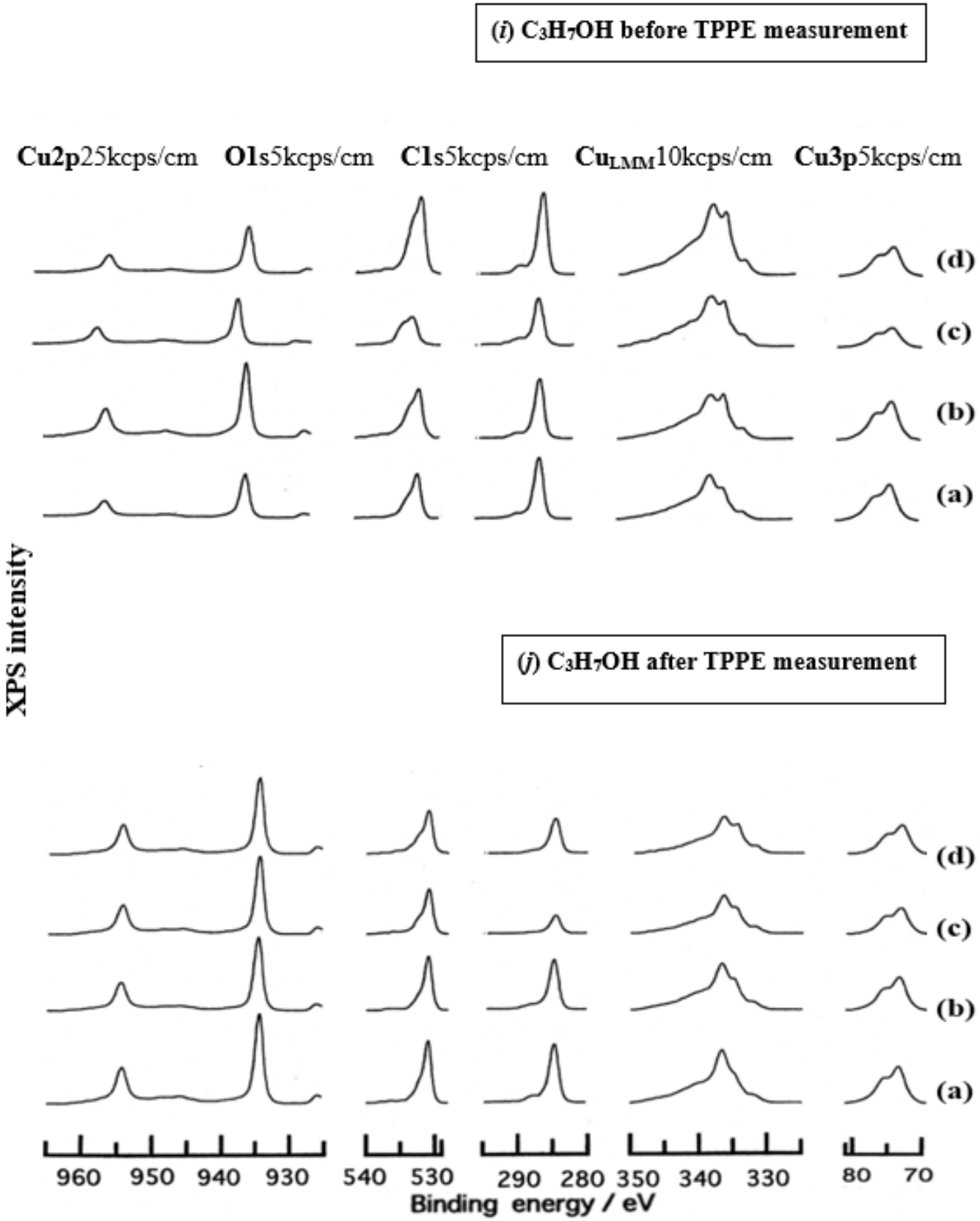

Figure 6. *Cont*.

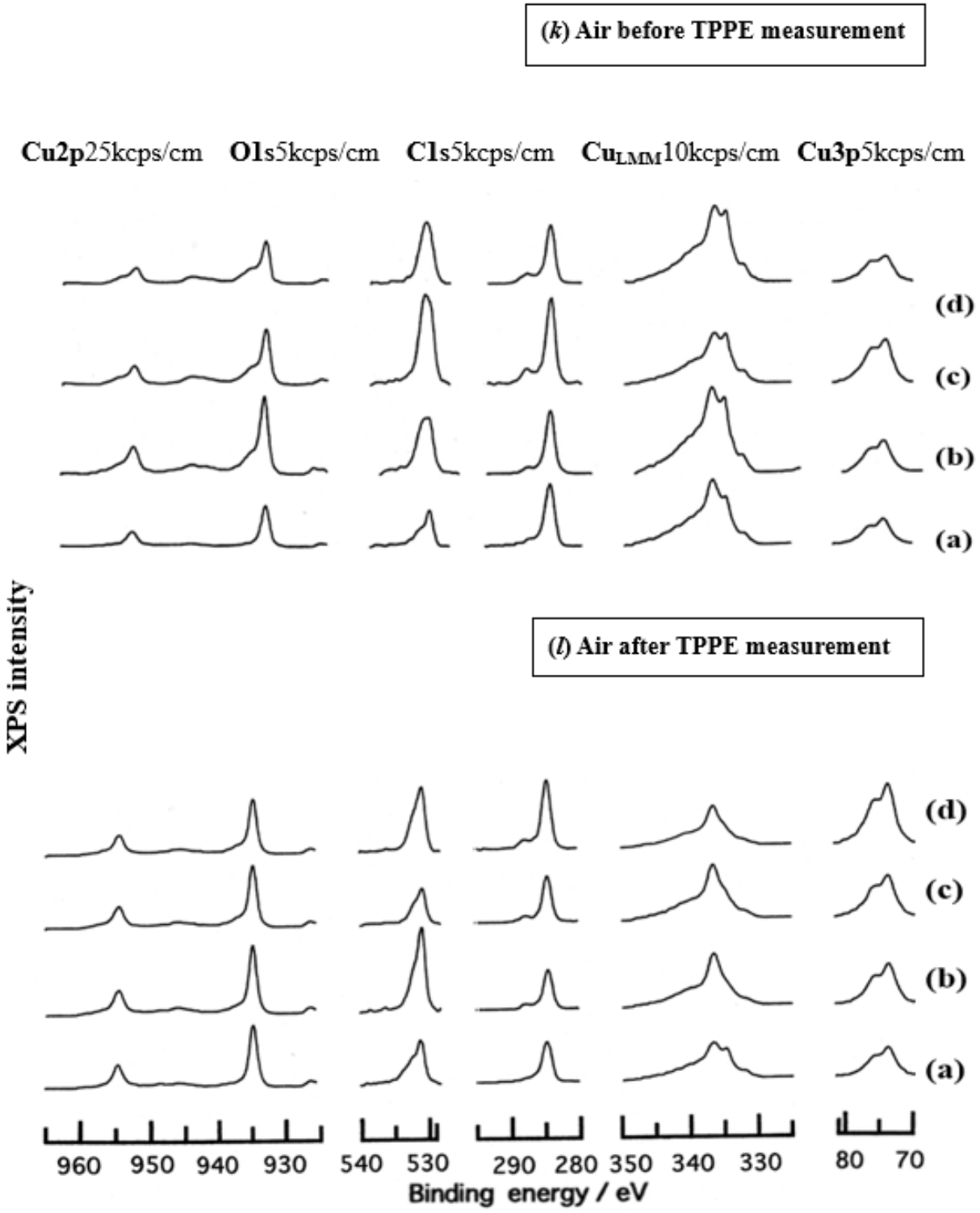

Figure 6. [Samples A and C] XPS spectra before and after TPPE measurement for copper sheets subjected to only ultrasonic cleaning in liquids and mechanical abrasion by a steel screw for certain periods in liquids and ambient air. Liquids and air: H_2O, CH_3OH, C_2H_5OH, $(CH_3)_2CHOH$, C_3H_7OH, and ambient air; (a) cleaned sample: after only ultrasonic cleaning for 5 min; (b–d) abraded samples: (b) 5-min abrasion; (c) 10-min abrasion; (d) 30-min abrasion. It should be noted that the intensities of each spectrum are represented by the unit of the length of 1 cm for the real output size.

The XPS spectra and characteristics are summarized as follows [26].

The atomic ratio of O1s/Cu2p for Cu ultrasonically cleaned alone in the liquids tended to decrease in the order $H_2O \approx CH_3OH > C_2H_5OH > (CH_3)_2CHOH \approx C_3H_7OH$. This may be related to the order of the amount of H_2O being adsorbed on the surfaces after cleaning in each liquid because the adsorption of H_2O most strongly decreases the N_T, as shown in Figure 5 (below). However, in the other cases, there was little relation between the N_T and the order of O1s/Cu2p and C1s/Cu2p.

The assignments of the XPS spectra before and after TPPE measurement in Figure 6 were conducted based on Refs. [30–33] and our previous reports [27,28]. The assignment of the XPS spectra on copper and oxygen is summarized as follows. The binding energy for the oxidation state of Cu is known as follows: 932.5 eV (Cu^0 and Cu^+) and 933.5 eV(Cu^{2+}) for Cu2p3/2; 335 eV (Cu^0) and 337 eV (Cu^+ and Cu^{2+}) for Cu_{LMM}; a strong shake-up satellite structure 6–10 eV above the main Cu2p peak in Cu^{2+} compounds. Concerning the Ols peak, Evans [31] suggested that two components appearing at 529.9 eV and 532.5 eV for the oxygen chemisorbed copper can be assigned to oxygen bonded directly to copper and oxygen adsorbed onto the initial Cu-O structure, respectively. McIntyre et al. [32] also suggested that the oxygen component of the higher binding energy component includes species such as OH, $Cu(OH)_2$, and H_2O. Recently, the XPS spectra of tarnished copper plates of phosphor bronze (C1220) (Cu purity: > 99.9%) were reported [33]. The binding energies of the Cu2p, the satellite, and O1s peaks were given as follows: Cu (932.6 eV), Cu_2O (932.7 eV), and CuO (933.1 eV) for the Cu2p peak; 943~948 eV (Cu_2O) and 940~945 eV (CuO) for the satellite peak; 531.7 eV ($Cu(OH)_2$), 530.7 eV (Cu_2O), and 529.8 eV (CuO) for the O1s peak [33].

In the Cu_{LMM}, spectra for every sample abraded and ultrasonically cleaned before the TPPE measurement shown in Figure 6, metallic Cu clearly appeared at 335 eV, but after the TPPE measurement, the metallic Cu greatly diminished for almost all samples. This finding suggested that the appearance of the metallic component before the TPPE measurement may be related to the increase in the PE intensity, but the detail of the mechanism remained unclear.

In the O1s peak shown in Figure 6, two components of $Cu(OH)_2$ and Cu_2O appearing at higher and lower binding energies, respectively, were preferential, but the CuO component was negligible. Regarding CuO, the reaction of $Cu_2O + (1/2)O_2 \rightarrow CuO$ is considered to be unlikely because of the lack of O_2 in the present experiment. The two components were observed for every sample before the TPPE measurement, but after the TPPE measurement, in almost all cases, the lower binding energy component became more preferential than the higher binding component, although samples of 10-minute abrasion in H_2O and ultrasonic cleaning in air both components were still preferential. This finding suggested that the change from the OH component (hydroxyl group) to the O^{2-} component (oxide ion) partially occurred being accompanied by the desorption of H_2O. Here, we suppose that this OH has a property of a radical, with the ability to attract electrons from the base metal through tunnelling followed by Auger emission, leading to the PE under light irradiation, although the mechanism of TPPE is not fully understood. We emphasize that this process becomes a key point in the increase in the TPPE intensity, as described later.

It was examined for clarification how the Cu2p3/2 and the satellite peaks can be associated with the adsorption of oxygen. Here, the binding energies for the observed spectra are represented by real measured values in the experiment. In Figure 6, for a sample of 10-minute abrasion in H_2O before the TPPE measurement, a sharp main Cu2p peak at 935 eV, which can be assigned to Cu and Cu_2O, and a broad shoulder peak at 937 eV in the higher binding energy region of the main Cu2p peak, which may originate from $Cu(OH)_2$, were observed, and the satellite peak was clearly observed at 940–948 eV, which may be originated from $Cu(OH)_2$ because the satellite grew with the increase in the shoulder peak. On the other hand, for a sample of ultrasonic cleaning in H_2O before the TPPE measurement shown in Figure 6, the sharp main peak was observed, but the satellite peak was very small. Similar behavior was observed for samples abraded in $(CH_3)_2CHOH$ and air before the TPPE measurement. In the case of samples abraded and ultrasonically cleaned in H_2O, $(CH_3)_2CHOH$, and air after the TPPE measurement, the satellite peak was very small, except for samples abraded in H_2O and ultrasonically cleaned in CH_3OH. For

both types of samples abraded and ultrasonically cleaned in C_2H_5OH and C_3H_7OH before and after the TPPE measurement, the satellite peak was almost negligible. This finding may suggest that the TPPE observed for C_2H_5OH and C_3H_7OH has little relation to the $Cu(OH)_2$ component as the source of the satellite appearing in Cu2p peak. Finally, it is considered that the chemical structure of the metal surfaces before the TPPE measurement is composed of adsorbate (alcohols, H_2O, and air)/$Cu(OH)_2$/Cu_2O/metallic Cu.

3.4. TPPE Characteristics for Sample A and Sample C and Their Relation to the Properties of Liquids

Figures 7 and 8 show Arrhenius plots of ln(N_Ta) and ln(N_Tc) vs. $1/T$ (K^{-1}) for sample A and sample C, respectively. TPPE characteristics for sample A and sample C are given in Tables 1 and 2, respectively.

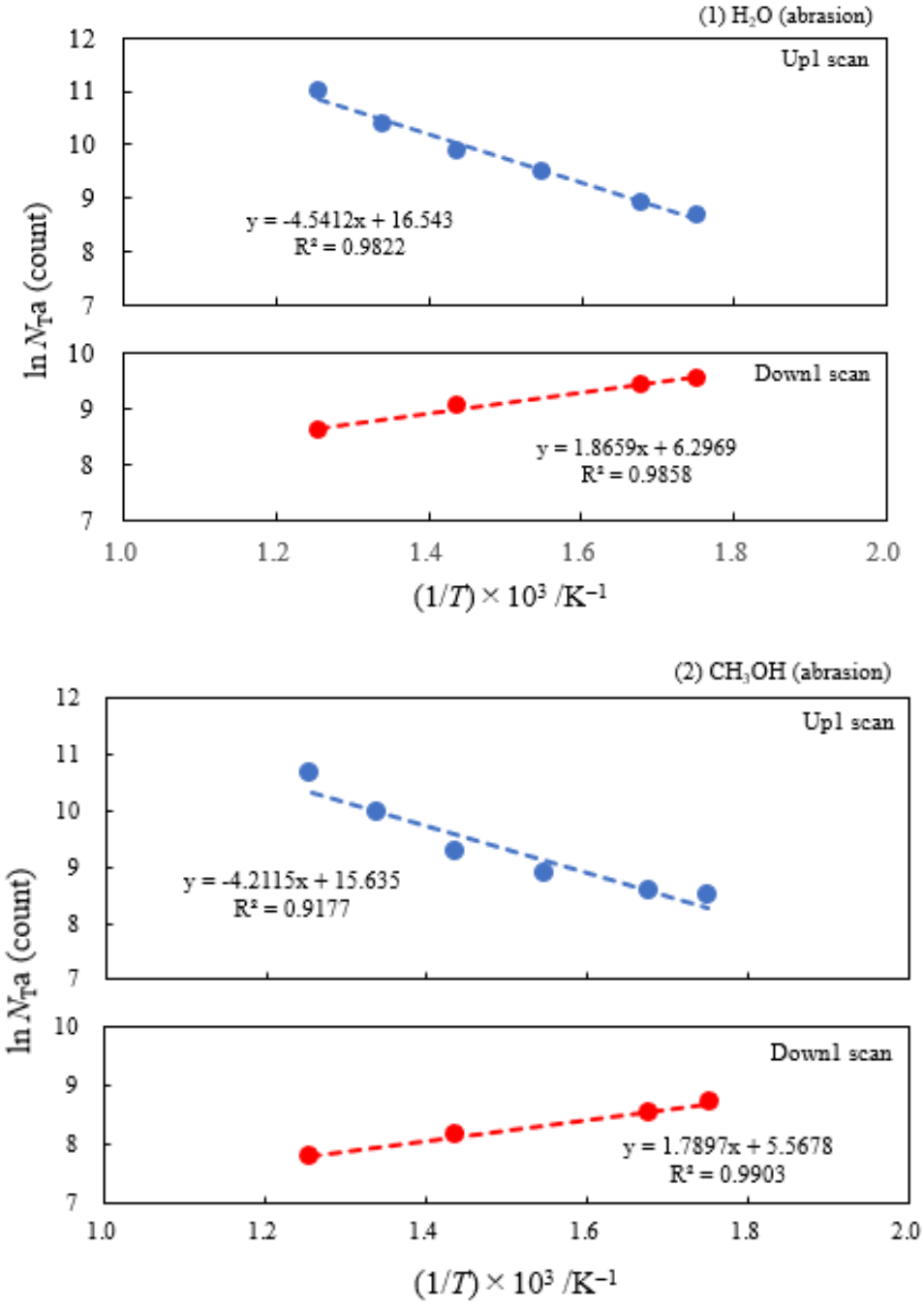

Figure 7. *Cont.*

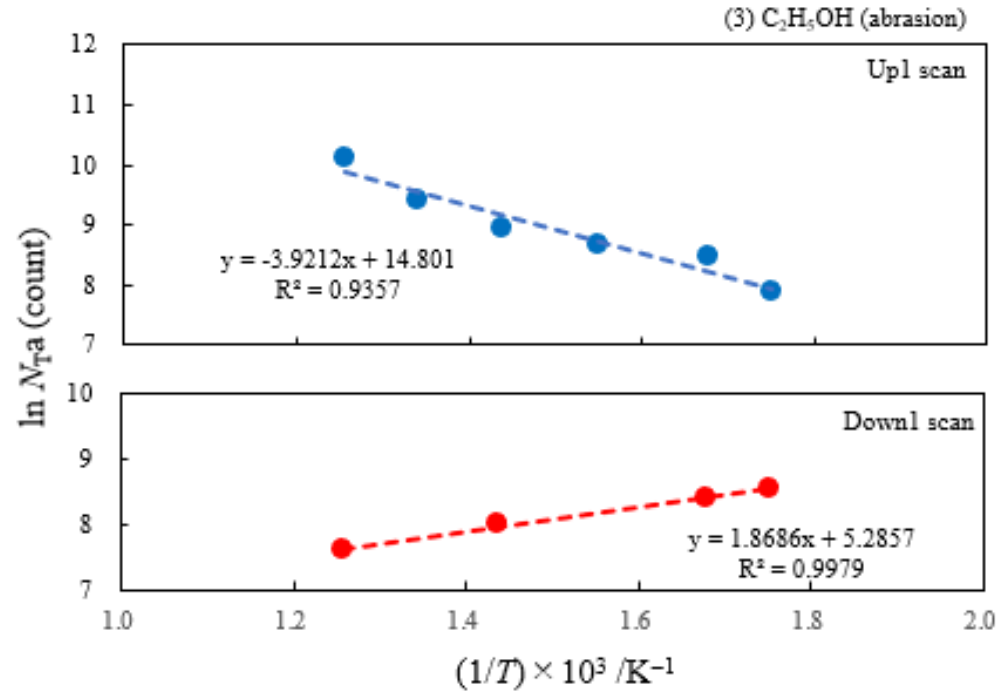

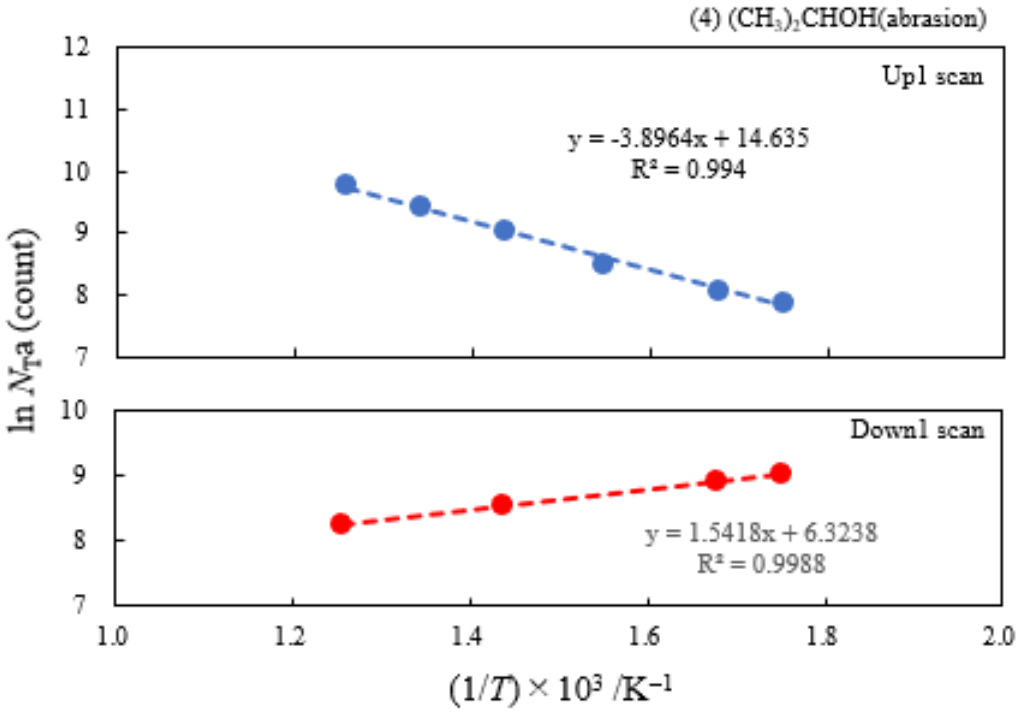

Figure 7. *Cont.*

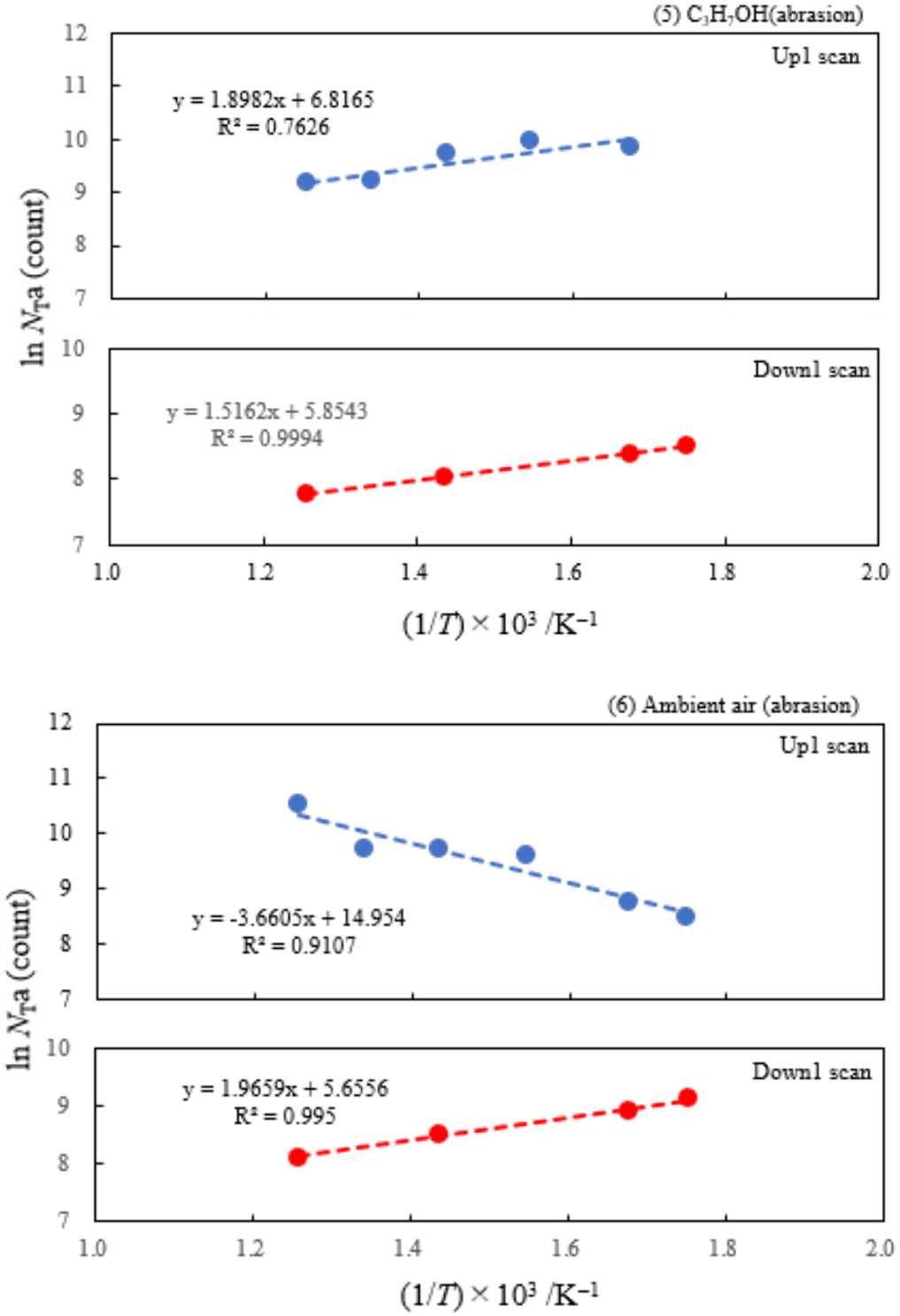

Figure 7. [Sample A] Arrhenius-type plots of ln(N_Ta) versus the reciprocal of measurement temperature ($1/T$) for copper samples abraded in liquids and air (Up1 scan is represented by blue line, and Down 1 scan is represented by red line) : (**1**) H_2O; (**2**) CH_3OH: (**3**) C_2H_5OH; (**4**) $(CH_3)_2HOH$; (**5**) C_3H_7OH; (**6**) ambient air. It is noted that the liquids are arranged in the decreasing order of the N_{Tmax}a. From the equation, represented by N_Ta = A_{0NT}a × exp(−ΔEa/kT), ΔEa and A_{0NT}a were obtained. The N_Ta values in the temperature range of 25–250 °C were used for Up1 and Down1 scans, representing the 1st temperature increase and subsequent temperature decrease processes, respectively.

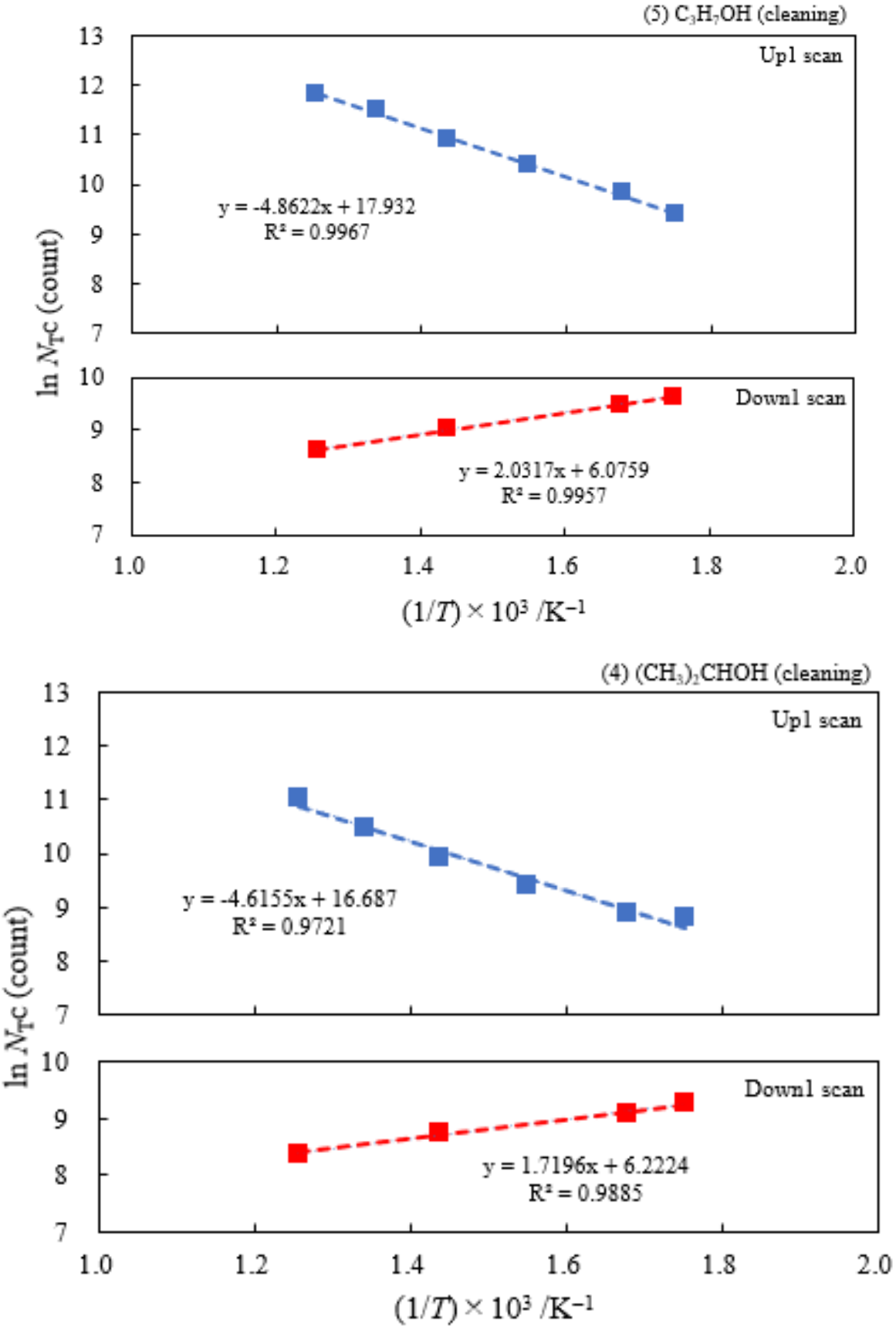

Figure 8. *Cont.*

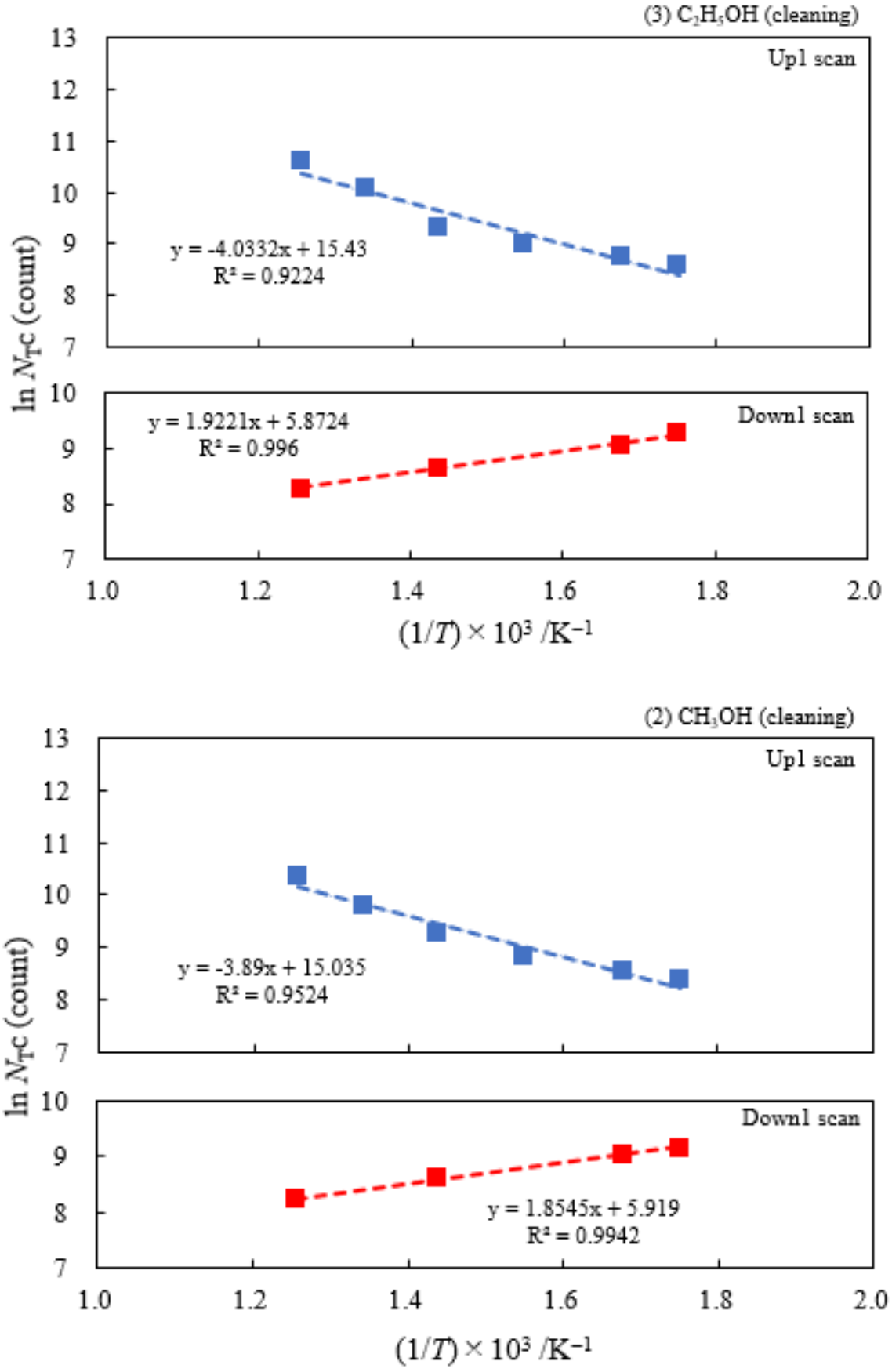

Figure 8. *Cont.*

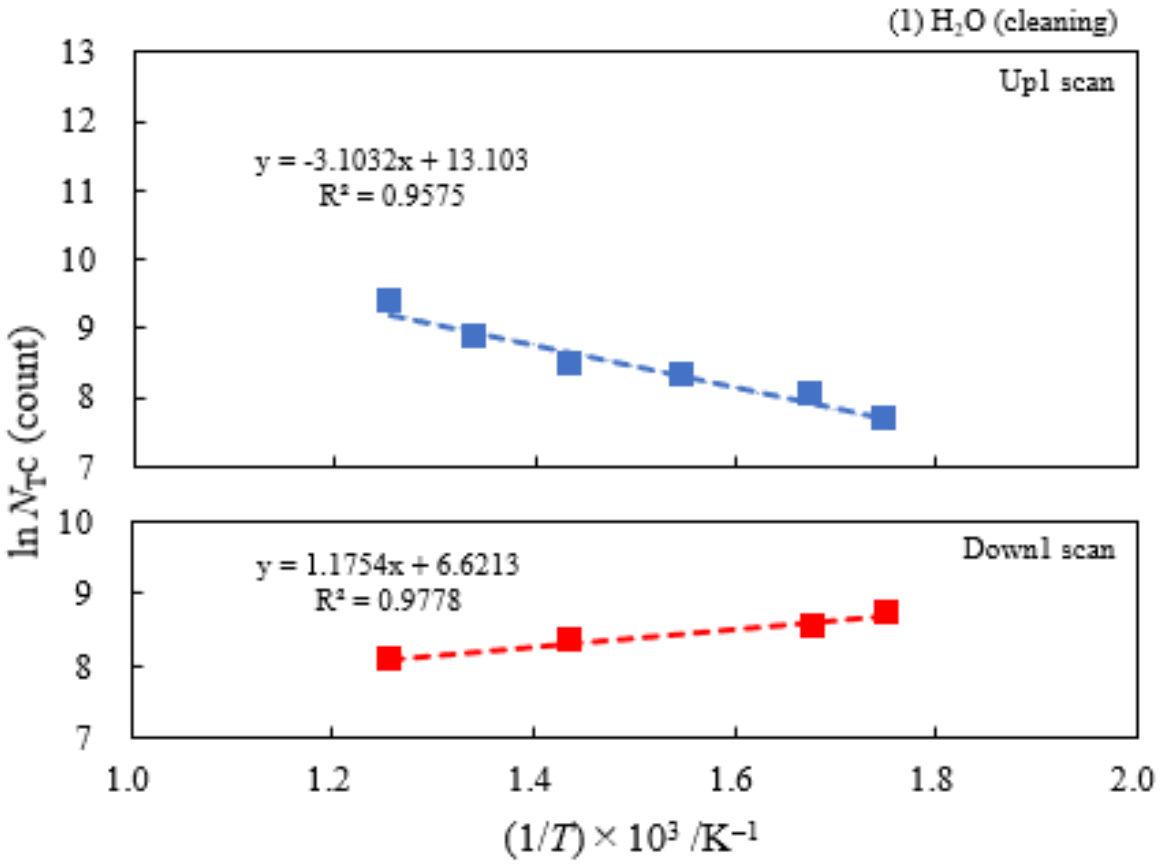

Figure 8. [Sample C] Arrhenius-type plots of ln(N_Tc) versus the reciprocal of measurement temperature ($1/T$) for copper samples subjected to ultrasonic cleaning in liquids: (**5**) C_3H_7OH; (**4**) $(CH_3)_2CHOH$; (**3**) C_2H_5OH; (**2**) CH_3OH; (**1**) H_2O. It is noted that the liquids are arranged in the decreasing order of the N_{Tmax}c. From the equation, represented by $N_T c = A_{0NT}c \times \exp(-\Delta Ec/kT)$, ΔEc and $A_{0NT}c$ were obtained. The N_Tc values in the temperature range of 25–250 °C were used for Up1 scan (blue line) and Down1 scan (red line), representing the 1st temperature increase and subsequent temperature decrease processes, respectively.

Table 1. [Sample A] Temperature-programmed photoelectron emission (TPPE) characteristics for copper sheets subjected to 10-minute abrasion in liquids and ambient air. Activation energy (ΔEa) and pre-exponential factor ($A_{0NT}a$) derived from the total number of emitted electrons (N_Ta) as a function of temperature and the maximum value of N_Ta (N_{Tmax}a) and its temperature (T_{max}a). The ΔEa and $A_{0NT}a$ values were obtained from the plots of the Arrhenius-type equation, $N_T a = A_{0NT}a \times \exp(-\Delta Ea/kT)$, versus measurement temperature. The N_Ta values in the temperature range of 25–250 °C were used for the plots. Up1 and Down1 indicate the 1st temperature increase and subsequent temperature decrease processes, respectively. Up2 and Down2 correspond to the 2nd temperature increase and subsequent temperature decrease processes after the 1st ones. The liquids from (1) to (4) are arranged in the decreasing order of N_{Tmax}a.

Liquids and Ambient Air as Environments Used for Abrading	**Maximum of N_Ta during the Up1 Process**	**Temperature of N_{Tmax}a during the Up1 Process**	**Activation Energy in 1st Temperature Increase Process**	**Activation Energy in 1st Temperature Decrease Process**	**Pre-Exponential Factor in 1st Temperature Increase Process**	**Activation Energy in 2nd Temperature Increase Process**	**Activation Energy in 2nd Temperature Decrease Process**
	$N_{Tmax}a/10^4$ count	$T_{max}a$/°C	ΔEa_{Up1}/eV	ΔEa_{Down1}/eV	$A_{0NT}a$/count	ΔEa_{Up2}/eV	ΔEa_{Down2}/eV
(1) Water	6.07	250	0.391	−0.161	1.53×10^7	−0.131	−0.214

Table 1. *Cont.*

Liquids and Ambient Air as Environments Used for Abrading	Maximum of N_Ta during the Up1 Process	Temperature of N_{Tmax}a during the Up1 Process	Activation Energy in 1st Temperature Increase Process	Activation Energy in 1st Temperature Decrease Process	Pre-Exponential Factor in 1st Temperature Increase Process	Activation Energy in 2nd Temperature Increase Process	Activation Energy in 2nd Temperature Decrease Process
(2) Methanol	4.18	250	0.363	−0.154	6.17×10^6		
(3) Ethanol	2.49	250	0.338	−0.161	2.68×10^6		
(4) 2-Propanol	1.73	250	0.336	−0.133	2.27×10^6		
(5) 1-Propanol [(a)]	2.12	100	−0.164	−0.131	9.13×10^2		
(6) Ambient air	3.70	250	0.315	−0.169	3.12×10^6		

[(a)] The N_Ta values in the Up1 scan increased with increasing temperature, passed through a maximum at the temperature of 100 °C, and then slowly decreased, reaching a constant level. In this case, the N_Ta values in the temperature range of 50–250 °C were used.

Table 2. [Sample C] Temperature-programmed photoelectron emission (TPPE) characteristics for copper sheets subjected to 5-min ultrasonic cleaning in liquids. Activation energy of photoelectron emission (ΔEc) and pre-exponential factor ($A_{0NT}c$) obtained from Arrhenius-type plots, $N_Tc = A_{0NT}c \times \exp(-\Delta Ec/kT)$, in the temperature range of 25–250 °C, using the total number of emitted electrons (N_Tc) as a function of temperature, and the maximum value of N_Tc ($N_{Tmax}c$) and its temperature ($T_{max}c$). The liquids are arranged in the decreasing order of $N_{Tmax}c$.

Liquids Used for Cleaning	Maximum of N_Tc during the Up1 Scan	Temperature of N_{Tmax}c during the Up1 Scan	Activation Energy in 1st Temperature Increase Process	Activation Energy in 1st Temperature Decrease Process	Pre-Exponential Factor in 1st Temperature Increase Process	Activation Energy in 2nd Temperature Increase Process	Activation Energy in 2nd Temperature Decrease Process
	$N_{Tmax}c/10^4$ count	$T_{max}c$/°C	ΔEc_{Up1}/eV	ΔEc_{Down1}/eV	$A_{0NT}c$/count	ΔEc_{Up2}/eV	ΔEc_{Down2}/eV
(5) 1-Propanol	13.2	250	0.419	−0.175	6.13×10^7	−0.158	−0.222
(4) 2-Propanol	6.21	250	0.398	−0.148	1.77×10^7		
(3) Ethanol	4.03	250	0.348	−0.166	5.03×10^6		
(2) Methanol	3.16	250	0.335	−0.160	3.39×10^6		
(1) Water	1.17	250	0.267	−0.101	4.90×10^5		

As shown in Table 3, the donor number (*DN*), as a measure of the basicity or donor ability of a solvent, and the acceptor number (*AN*), which measures the electrophilic behavior of a solvent, defined by Gutmann, are given for the liquids. There is no exact correlation between donor number (*DN*) and dielectric constant. However, in Figure 9, it can be confirmed that the reciprocal of dielectric constant ($\varepsilon/\varepsilon_0$) tends to linearly decrease with increasing acceptor number (*AN*) of the liquids. Although the reason for this relation remains unclear, this observation suggests that *AN* can be strongly related to the electrostatic interaction; that is, the ability of the liquids to accept electron works great in the adsorption. Further, this suggests that the effect of electric charges in liquids with a higher value of *AN* is small. Scheme 1 shows the solvation of triethylphosphine oxide $(C_2H_5)_3P{=}O$ by solvent molecule (S) and its correspondence to the adsorption of the alcohols and water on the surface hydroxyl group (−Cu-OH). Abe at al. [34] reported the relationship between the charge distribution on P and O atoms in triethylphosphine oxide–solvent molecule, the P–O bond distance, and the hydrogen bond distance between triethylphosphine oxide–solvent molecule and the *AN* value of solvents. According to Ref. [34], the charge distribution on P and O atoms can be changed by adsorption of solvent molecule with *AN*. The charge distribution on the P atom decreases, while that of the O atom increases with increasing *AN* value. The P–O bond distance increases, while the hydrogen bond between triethylphosphine oxide–solvent molecule decreases with increasing *AN*. Relating these results to the

present study, it is considered that the negative charge of the oxygen atom of the surface hydroxyl group may be increased due to the electrostatic interaction with the liquids with high *AN*.

Table 3. Relation between acceptor number, donor number, and dielectric constant of liquids.

Liquids Used for Abrading and Ultrasonic Cleaning	Acceptor Number [a]	Donor Number [a]	Dielectric Constant (25 °C) [c]	Reciprocal of Dielectric Constant
	AN	*DN*	$\varepsilon/\varepsilon_0$	$1/(\varepsilon/\varepsilon_0)$
(1) Water (H_2O)	54.8	18.0	78.39	0.0128
(2) Methanol (CH_3OH)	41.3	20.0	32.70	0.0306
(3) Ethanol (C_2H_5OH)	37.1	19.0	24.55	0.0407
(4) 2-Propanol $(CH_3)_2CHOH$	33.5 [b]	21.1 [b]	19.92	0.0502
(5) 1-Propanol (C_3H_7OH)			20.33	0.0492

[a] Huheey, J. E. *in Inorganic Chemistry, Principles of Structure and Reactivity*, 3rd edn. Harper & Row, New York (1983). Japanese translation by Kodama, G; Nakazawa, H. Tokyo Kagaku Dojin (Tokyo, 1984), pp. 340–341 [35]. [b] http://www.stenutz.eu/chem/solv21.php (accessed on 5 January, 2024) [36]. [c] Riddick, J. A.; Bunger, W. B. *Organic Solvents*, 3rd edn. Wiley-Interscience, New York (1970) [37].

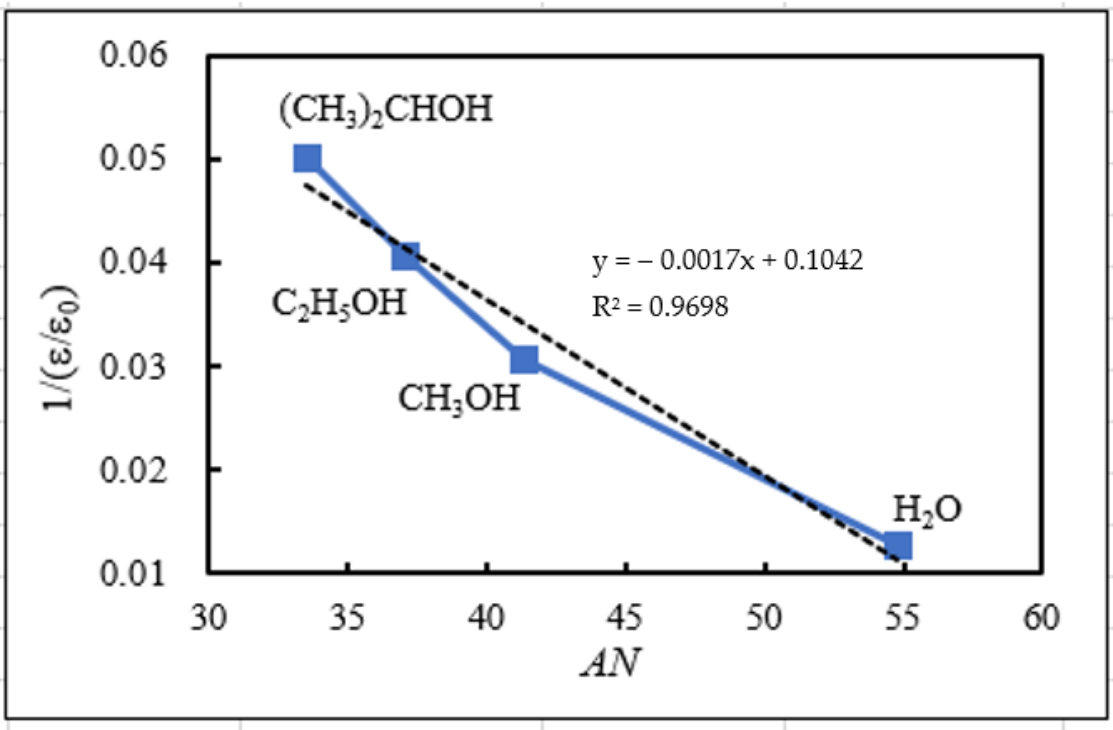

Figure 9. Relation between the reciprocal of dielectric constant ($\varepsilon/\varepsilon_0$) and acceptor number (*AN*) of the liquids.

Figures 10 and 11 show the relation between the TPPE characteristics and the properties of the liquids: N_{Tmax}a, ΔEa_{Up1}, *AN*, and $1/\varepsilon/\varepsilon_0$ for sample A, and N_{Tmax}c, ΔEc_{Up1}, *AN*, and $1/\varepsilon/\varepsilon_0$ for sample C, respectively. At first, in Figure 12, we consider the adsorption of the molecules of alcohols and water on the surface hydroxyl group (Cu–OH) at the surface. It should be noted that $Cu(OH)_2$ has been reported to play an initial key role in growth of the corrosion layer [25]. We consider that the acid–base property of Cu–OH can be determined by the electron density of the oxygen atom of the Cu–OH on the surface. We think that the oxide film of sample A is much thinner than that of sample C. Due to the bias of the negative potential and the light irradiation during the TPPE measurement, it is

considered that the electron density of the oxygen of sample A is low, but that of sample C is high, with the former acting as an acid and the latter as a base.

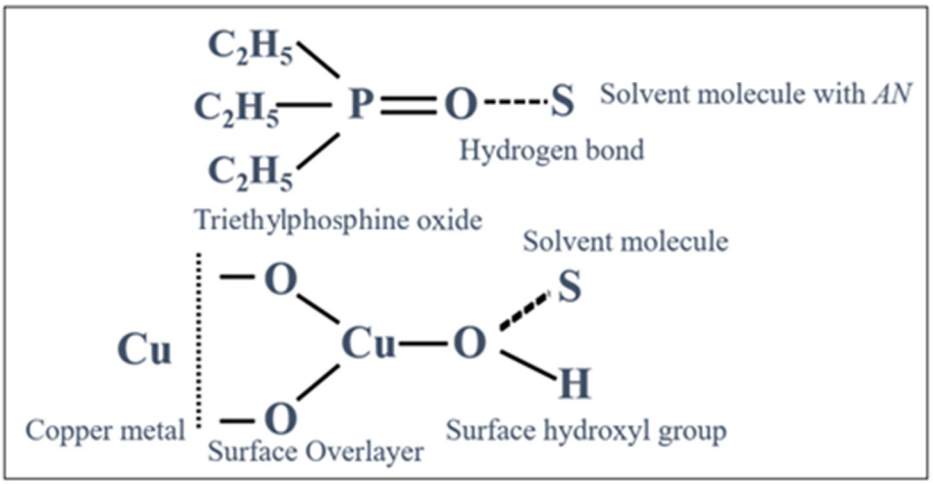

Scheme 1. The solvation between triethylphosphine oxide $(C_2H_5)_3P{=}O$ and solvent molecule (S), changing charge distribution on P and O atoms and its correspondence to the adsorption of the alcohols and water on the surface hydroxyl group (−Cu-OH).

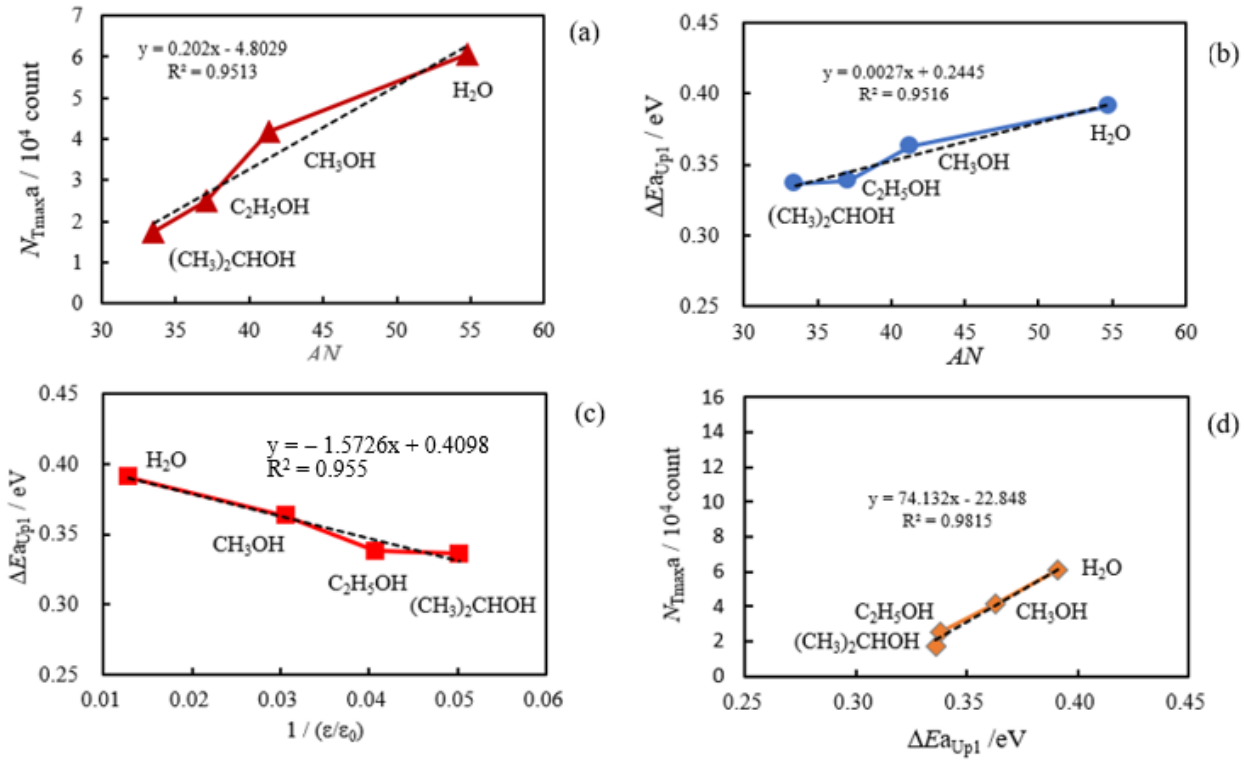

Figure 10. [Sample A] TPPE characteristics of copper sheets subjected to 10-minute abrasion in liquids and the property of liquids: (**a**) relation between the maximum value of N_Ta (N_{Tmax}a) during the Up1 scan and the acceptor number (*AN*) of the liquids; (**b**) relation between the activation energy of photoelectron emission (ΔEa_{Up1}) during Up1 scan and the acceptor number (*AN*) of the liquids; (**c**) relation between ΔEa_{Up1} and the reciprocal of dielectric constant ($\varepsilon/\varepsilon_0$) of the solvents; (**d**) relation between the value of N_{Tmax}a and ΔEa_{Up1}. The data come from Table 1. We used the same color lines in (**a**–**d**) of Figures 10 and 11 for comparison.

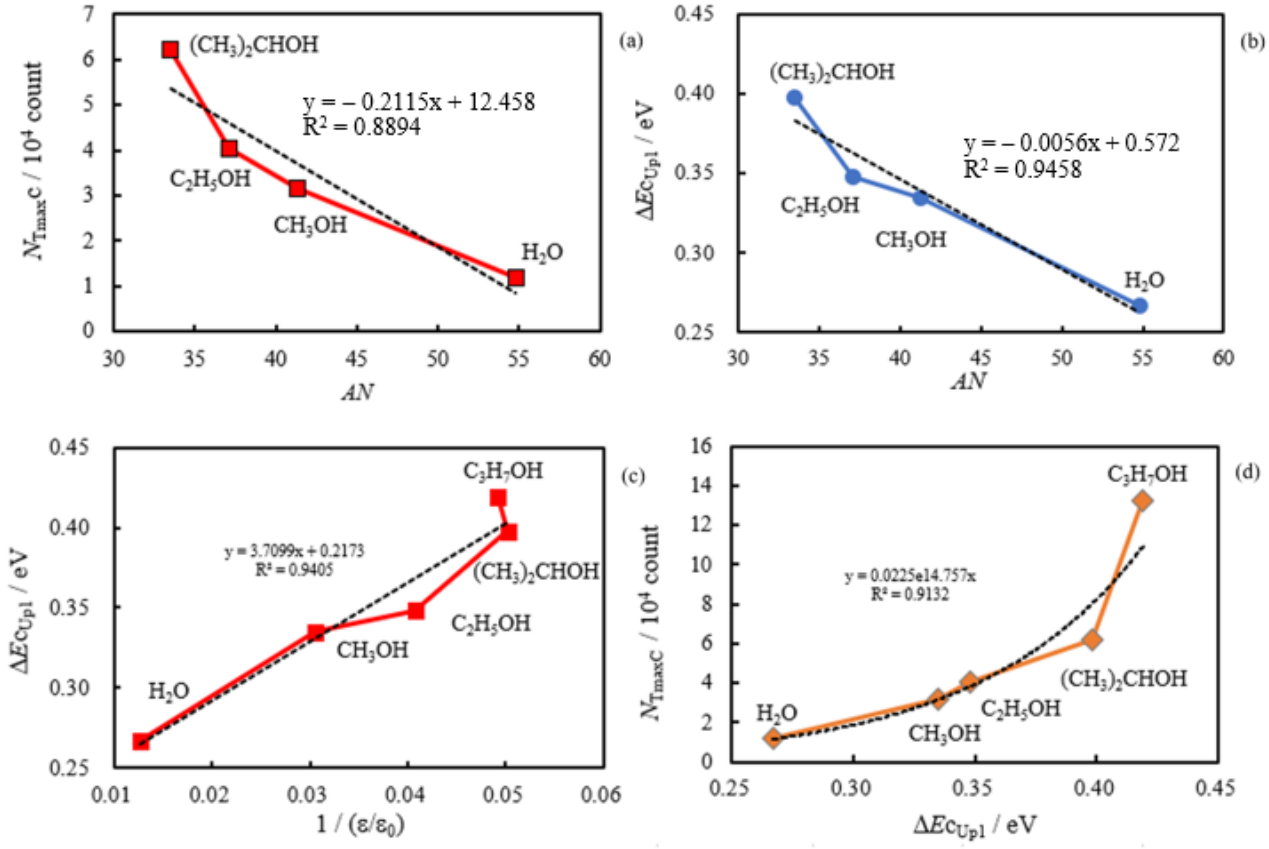

Figure 11. [Sample C] TPPE characteristics of copper sheets subjected to 5-minute ultrasonic cleaning in the liquids and the property of the liquids: (**a**) relation between the maximum value of N_{Tc} ($N_{Tmax}c$) and the acceptor number (*AN*) of the liquids; (**b**) relation between ΔEc_{Up1} and *AN* of the liquids; (**c**) relation between ΔEc_{Up1} and the reciprocal of dielectric constant ($\varepsilon/\varepsilon_0$) of the liquids; (**d**) relation between the value of $N_{Tmax}c$ during Up1 scan and ΔEc_{Up1}. The data come from Table 2.

As a result, the –Cu–OH of sample A more strongly interacts with more basic liquid molecules, while that of sample C more strongly acts with more acidic liquid molecules. Figure 12 shows the orientation of the electric dipole produced by the adsorbed molecule. For the property of the liquids, we used Gutmann's acceptor number (*AN*), representing the basicity of the liquid molecules: $(CH_3)_2CHOH$ (33.5), C_2H_5OH (37.1), CH_3OH (41.3), and H_2O (54.8). This was well related to the TPPE characteristics. With sample A, the values of $N_{Tmax}a$ and ΔEa_{Up1} both increased with increasing *AN* (Table 1 and Figure 10). On the other hand, with sample C, the values of $N_{Tmax}c$ and ΔEc_{Up1} both decreased with increasing *AN* (Table 2 and Figure 11). Interestingly, the characteristics of the TPPE for sample A and sample C are correlated with *AN* and $1/(\varepsilon/\varepsilon_0)$ of the liquids, but take completely opposite trends. In Figures 10 and 11, the relation of $N_{Tmax}a$ vs. *AN*, ΔEa_{Up1} vs. *AN*, and ΔEa_{Up1} vs. $1/\varepsilon/\varepsilon_0$ for sample A is completely opposite to that of $N_{Tmax}c$ vs. *AN*, ΔEc_{Up1} vs. *AN*, and ΔEc_{Up1} vs. $1/\varepsilon/\varepsilon_0$ for sample C. However, in Figures 10 and 11, it is seen that the relation of $N_{Tmax}a$ vs. ΔEa_{Up1} is similar to that of $N_{Tmax}c$ vs. ΔEc_{Up1}, although the order of the liquids at the data points is opposite. It remains unclear why N_{Tmax} increases with increasing ΔE_{Up1}.

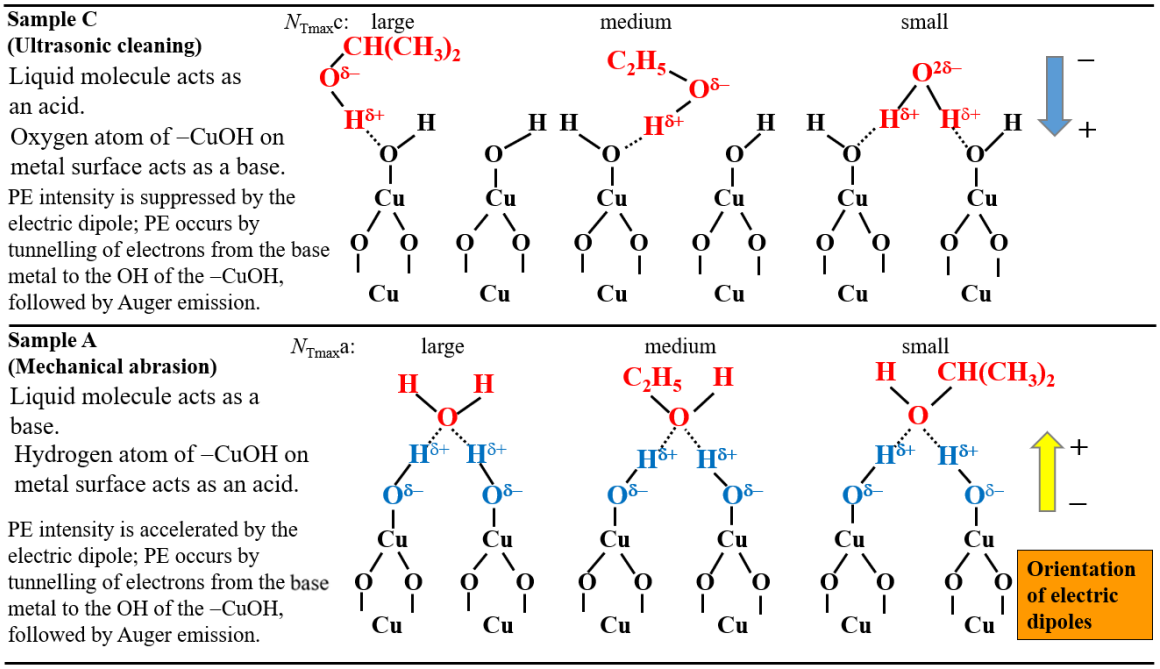

Figure 12. Examples of the acid–base interaction modes between the molecules of $(CH_3)_2CHOH$, C_2H_5OH, and H_2O and the surface hydroxyl group (–CuOH) and the orientation of the formed electric dipoles for sample C and sample A. These interaction modes have been reported by the author. The hydroxyl groups present at the overlayer are represented by black letters (Sample C) and blue letters (Sample A). In Sample C, the H atom of the hydroxyl group of the liquid molecule is bonded to the lone pair of the O atom of the –CuOH, forming the hydrogen bond and the electric dipole with a negative pole outside. In Sample A, the H atom pf the –CuOH is bonded to the lone pair of the O atom of the adsorbed liquid molecule, generating the hydrogen bond and the electric dipole with the positive pole outside. The electron density of the O atom of –CuOH is considered to play an essential role in the acid–base interaction.

In Refs. [4,5], regarding contact killing, it is reported that a few general principles appear to be clear: higher copper content of alloys, higher temperature, and higher relative humidity increased the efficacy of contact killing. The temperature and water adsorption dependence of the photoelectron emission behavior observed in the TPPE experiment may be related to the efficacy of contact killing by metallic Cu.

3.5. TPPE Mechanism and Its Relation to Activation Energy

We propose a model of PE based on the tunnelling of electrons to the hydroxyl group radical (the formula of –Cu-OH• is used to emphasize the radical), followed by Auger emission, and further, the activation energy of PE, which is provided by the heat produced when –Cu-OH• attracts electrons from the base metal. Ramsey [38] emphasized that a model for exoemission due to the chemisorption of electronegative gases on metals based on electron tunnelling followed by Auger emission is very promising.

The reason why we adopt the electron tunnelling model is described as follows. A reactive hydroxyl radical (OH•) can be generated in a Fenton-type reaction [4,6]. The OH• radical has a relatively great tendency to attract electrons to itself. This radical can be considered as one of the electronegative gases. The electron affinity of OH is reported to be 1.83 eV [39]. In Figure 10d, for sample A, we described that the N_{Tmax}a values increase with increasing ΔEa_{Up1} in the 1st temperature increase process. This relationship is completely inconsistent with the observation that the total count of electrons emitted during the Up1 scan decreases with increasing activation energy (ΔE_{Up1}) for scratched Fe surfaces in Figure 10 of Ref. [40]. This suggests that the PE mechanism in the copper surfaces is more complicated. We think that the activation energies in the present copper surfaces cannot be

explained by the *ET* taking place over the energy barrier of the overlayer. A key reaction step on the surface during the TPPE measurement is represented by the partial change in the O1s spectra from an OH component ($Cu(OH)_2$) to an O^{2-} component (Cu_2O).

The reason why we adopt the electron tunnelling model is described as follows. A reactive hydroxyl radical ($OH^{\bullet}$) can be generated in a Fenton-type reaction [4,6]. The $OH^{\bullet}$ radical has a relatively great tendency to attract electrons to itself. This radical can be considered as one of the electronegative gases. The electron affinity of OH is reported to be 1.83 eV [39]. In Figure 10d, for sample A, we described that the $N_{Tmax}a$ values increase with increasing ΔEa_{Up1} in the 1st temperature increase process. This relationship is completely inconsistent with the observation that the total count of electrons emitted during the Up1 scan decreases with increasing activation energy (ΔE_{Up1}) for scratched Fe surfaces in Figure 10 of Ref. [37]. This suggests that the PE mechanism in the copper surfaces is more complicated. We think that the activation energies in the present copper surfaces cannot be explained by the *ET* taking place over the energy barrier of the overlayer. A key reaction step on the surface during the TPPE measurement is represented by the partial change in the O1s spectra from an OH component ($Cu(OH)_2$) to an O^{2-} component (Cu_2O).

Figure 13 shows a simple energy level diagram based upon electron tunnelling to adsorbed hydroxyl radicals followed by Auger emission. According to the review of atmospheric corrosion [25], the chemical reactions can be represented by Equations (1)–(4):

$$Cu + H_2O + (1/2)O_2 \rightarrow Cu(OH)_2 \quad (1)$$

$$Cu(OH)_2 \rightarrow H_2O + CuO \quad (2)$$

$$Cu + CuO \rightarrow Cu_2O \quad (3)$$

$$Cu_2O + (1/2)O_2 \rightarrow CuO \quad (4)$$

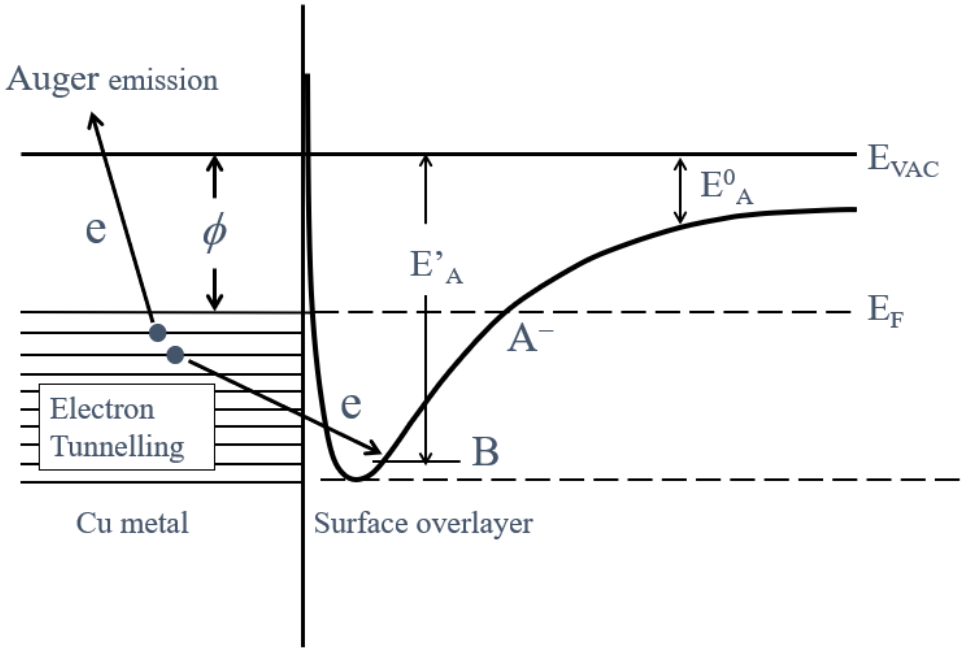

Figure 13. A simple energy level diagram based upon electron tunnelling to the trap (B) of the adsorbed hydroxyl radical (B) followed by Auger emission. The depth of the trap increases in the order $(CH_3)_2CHOH < C_2H_5OH < CH_3OH < H_2O$ for sample A and $H_2O < CH_3OH < C_2H_5OH < (CH_3)_2CHOH < C_3H_7OH$ for sample C; φ work function; $E^0{}_A$ (electron affinity for OH alone) = 1.83 eV; E'_A, electron affinity of OH adsorbed on the Cu surface in the liquids; E_F, Fermi level. The two types of electrons for tunnelling to the surface hydroxyl group and for Auger emission from Fermi level, producing PE are represented by two letters of e.

In the thin film on the sample surface during the TPPE measurement, referring to the XPS results shown in Figure 6, Equations (1)–(3) play an essential role in producing OH and O^{2-}, where the Cu shows the route where the initial Cu atom is successively involved in these reactions. Equation (4) is not considered. The $OH^{\bullet}$ radical may be created at the spot composed of Cu, $Cu(OH)_2$, and CuO under light irradiation. This situation may be represented by the electron affinity curve of the negative ion of $OH^{\bullet}$ approaching close to the surface under the control of the image force. We consider that the tunnelling of electrons at the Fermi level of the base metal to the OH trap level is to attract electrons, produces heat in the same way as heat of adsorption used in surface chemistry. The depth of the trap level is influenced by the acid–base interaction of the liquids adsorbed near the OH. The produced heat as well as the irradiated light excites electrons from the Fermi level, leading to the PE stimulation spectrum. The activation energies obtained from the TPPE measurement correspond to the depth of the trap level.

3.6. TPPE in the Down1, Up2, and Down2 Scan Processes and Activation Energy

The TPPE plots during all of the temperature scan processes for sample A and sample C are shown in Figures 3 and 4, respectively. The values of ΔEa_{Down1}, ΔEa_{Up2}, and ΔEa_{Down2} for sample A, and ΔEc_{Down1}, ΔEc_{Up2}, and ΔEc_{Down2} for sample C are given in Tables 1 and 2, respectively. It is seen that these values are negative and almost independent of the liquids, and further, the absolute values of ΔE_{aDown1} were considerably smaller than those of ΔE_{aUp1}. Regarding the electrical resistance (ρ, ohm-cm) of Cu_2O (p-type semiconductor), it was reported that the electrical resistance increases with decreasing temperature [41]. From the data of the electrical resistance in Figure 13.3 of Ref. [41], we obtained the activation energy of −0.774 eV by applying an Arrhenius plot. On the other hand, the conductivity (σ) of Cu_2O was investigated by Juse and Kurtschatow [42]. These authors found that the conductivity increases with the increasing oxygen content of Cu_2O. It was found that the conductivity of Cu_2O can be represented by Formula (5):

$$\sigma = A_1 e^{-\varepsilon 1}/kT + A_2 e^{-\varepsilon 2}/kT \quad (5)$$

where ε_1 = 0.7 eV, $A_1 \sim 100$ $cm^{-1}\cdot ohm^{-1}$, both being independent of the oxygen content, and ε_2 varies between 0.129 and 0.134 eV, while A_2 depends strongly on the oxygen content. For specimens with about 0.1% of weight of excess oxygen, $A_2 \sim 0.3$ $cm^{-1}\cdot ohm^{-1}$. These authors suggested that the first term represents the conductivity of pure Cu_2O, and that the second term represents the conductivity due to excess oxygen [42,43]. In the present TPPE experiment, we think that the adsorbates on the sample surface were fully desorbed by the temperature increase scan to 350 °C, leaving adsorbed oxygen. Compared to the activation energies of the electrical resistance of −0.774 eV in Ref. [41] and of the conductivity of ε_1 = 0.7 eV [42,43], it is seen that the experimental values of TPPE obtained in the present experiment are remarkably small: for sample A, ΔEa_{Down1} varies between −0.131 and −0.161 eV, ΔEa_{Up2} = −0.131 eV, and ΔEa_{Down2} = −0.214 eV; for sample C, ΔEc_{Down1} varies between −0.101 and −0.175 eV, ΔEc_{Up2} = −0.158 eV, and ΔEc_{Down2} = −0.222 eV. We consider that the PE in the Down1, Up2, and Down2 scan processes can be controlled by the electrical resistance or the conductivity of the overlayer. Therefore, it is thought that the small activation energy values may be due to excess oxygen content in the Cu_2O formed on the copper surfaces.

4. Conclusions

This study is summarized as follows: (a) the distinguishment of the TPPE data during the temperature increase process of the Cu surfaces subjected to different treatments was re-examined. (b) The effects of adsorbed alcohols and water and mechanical abrasion on TPPE were distinguished. (c) The maximum total count of emitted electrons was correlated with the activation energies for the electron emission using the TPPE data. (d) The relationship of the TPPE data was explained by Gutmann's acceptor number (*AN*) of the liquids. (e) A mechanism of TPPE from Cu through the tunnelling of electrons in the metal to the surface

hydroxyl group, followed by Auger emission, was proposed. (f) The involvement of the OH component of the O1s spectra in TPPE was emphasized. (g) The electrons produced in this way have the ability to move around in the surface overlayer, maybe functioning in the inactivation of viruses. (h) The TPPE measurement during the first temperature decrease and second temperature increase and subsequent temperature decrease processes was examined.

Funding: This research received no external funding.

Institutional Review Board Statement: Not applicable.

Informed Consent Statement: Not applicable.

Data Availability Statement: The data presented in this study are available on request from the corresponding author. The data are not publicly available due to privacy.

Acknowledgments: The author gratefully acknowledges Masakazu Honma and Suguru Kohno, who were the former students of the author, for performing the experiments and measurements of TPPE and XPS.

Conflicts of Interest: The author declares no conflicts of interest.

References

1. Momose, Y. *Exoemission from Processed Solid Surfaces and Gas Adsorption*; Springer Series in Surface Sciences; Springer: Berlin/Heidelberg, Germany, 2023. [CrossRef]
2. Morrison, J. Copper's Virus-Killing Powers Were Known Even to the Ancients. COVID-19 a Smithsonian Magazine Special Report. 14 April 2020. Available online: https://www.smithsonianmag.com/science-nature/copper-virus-kill-180974655/ (accessed on 14 April 2020).
3. Tian, H.; He, B.; Yin, Y.; Liu, L.; Shi, J.; Hu, L.; Jiang, G. Chemical nature of metals and metal-based materials in inactivation of viruses. *Nanomaterials* **2022**, *12*, 2345. [CrossRef] [PubMed]
4. Grass, G.; Rensing, C.; Solioz, M. Metallic copper as an antimicrobial surface. *Appl. Environ. Microbiol.* **2011**, *77*, 1541–1547. [CrossRef] [PubMed]
5. Elguindi, J.; Moffitt, S.; Hasman, H.; Andrade, C.; Raghavan, S.; Rensing, C. Metallic copper corrosion rates, moisture content, and growth medium influence survival of copper-ion resistant bacteria. *Appl. Microbiol. Biotechnol.* **2011**, *89*, 1963–1970. [CrossRef] [PubMed]
6. Scully, J.R. The COVID-19 Pandemic, Part 1: Can antimicrobial copper-based alloys help suppress infectious transmission of viruses originating from human contact with high-touch surfaces? *Corrosion* **2020**, *76*, 523–527. [CrossRef] [PubMed]
7. Hans, M.; Erbe, A.; Mathews, S.; Chen, Y.; Solioz, M.; Mücklich, F. Role of copper oxides in contact killing of bacteria. *Langmuir* **2013**, *29*, 16160–16166. [CrossRef] [PubMed]
8. Hans, M.; Mathews, S.; Mücklich, F.; Solioz, M. Physicochemical properties of copper important for its antibacterial activity and development of a unified model. *Biointerfaces* **2016**, *11*, 018902. [CrossRef]
9. Luo, J.; Hein, C.; Mücklich, F.; Solioz, M. Killing of bacteria by copper, cadmium, and silver surfaces reveals relevant physicochemical parameters. *Biointerfaces* **2017**, *12*, 020301. [CrossRef]
10. Minoshima, M.; Lu, Y.; Kimura, T.; Nakano, R.; Ishiguro, H.; Kubota, Y.; Hashimoto, K.; Sunada, K. Comparison of the antiviral effect of solid-state copper and silver compounds. *J. Hazard. Mater.* **2016**, *312*, 1–7. [CrossRef]
11. Mallakpour, S.; Azadi, E.; Hussain, C.M. The latest strategies in the fight against the COVID-19 pandemic: The role of metal and metal oxide nanoparticles. *New J. Chem.* **2021**, *45*, 6167. [CrossRef]
12. Wang, Y.; Wang, Q.; Wu, G.; Xiang, H.; Innocent, M.T.; Zhai, M.; Jia, C.; Zou, P.; Zhou, J.; Zuu, M. Ultra-fast bacterial inactive tion of Cu_2O@halloysite nanotubes hybrids with charge adsorption and physical piercing ability for medical protective fabrics. *J. Mater. Sci. Technol.* **2022**, *122*, 1–9. [CrossRef]
13. Delong, Z.; Maimaiti, H.; Awati, A.; Yisilamu, G.; Fengchang, S. Synthesis and photocatalytic CO_2 reduction performance of Cu_2O.Coal-based carbon nanoparticle composites. *Chem. Phys. Lett.* **2018**, *16*, 27–35. [CrossRef]
14. Shimabukuro, M.; Manaka, T.; Tsutsumi, Y.; Nozaki, K.; Chen, P.; Ashida, M.; Nagai, A.; Hanawa, T. Corrosion Behavior and Bacterial Viability on Different Surface States of Copper. *Mater. Trans.* **2020**, *61*, 1143–1148. [CrossRef]
15. Champagne, V.K.; Helfritch, D.J. A demonstration of the antimicrobial effectiveness of various copper surfaces. *J. Biol. Eng.* **2013**, *7*, 8. [CrossRef] [PubMed]
16. Bryce, E.A.; Velapatino, B.; Khorami, H.A.; Donnelly-Pierce, T.; Wong, T.; Dixon, R.; Asselin, E. In vitro evaluation of antimicrobial efficacy and durability of three copper surfaces used in healthcare. *Biointerphases* **2020**, *15*, 011005. [CrossRef] [PubMed]
17. Sousa, B.C.; Cote, D.L. Antimicrobial copper cold spray coatings and SARS-CoV-2 surface inactivation. *MRS Adv.* **2020**, *5*, 2873–2880. [CrossRef] [PubMed]

18. Chen, C.; Li, Y.; Bao, R.; Yang, L.; Cui, M.; Cheng, S.; Liu, J.; Xia, J. CuxO@Cu mesh electrode with {1 1 1} facet for efficient photo-electro-Fenton reaction and low voltage robustness. *Appl. Surf. Sci.* **2023**, *626*, 157187. [CrossRef]
19. Thomas, N.; Dionysiou, D.D.; Pillai, S.C. Heterogeneous Fenton catalysis: A review of recent advances. *J. Hazard. Mater.* **2021**, *404*, 124082. [CrossRef]
20. Yao, Y.; Pan, Y.; Yu, Y.; Yu, Z.; Lai, L.; Liu, F.; Wei, L.; Chen, Y. Bifunctional catalysis for heterogeneous electro-Fenton processes: A review. *Environ. Chem. Lett.* **2022**, *20*, 3837–3859. [CrossRef]
21. Cross, J.B.; Currier, R.P.; Torraco, D.J.; Vanderberg, L.A.; Wagner, G.L.; Gladen, P.D. Killing of Bacillus Spores by aqueous dissolved oxygen, ascorbic acid, and copper ions. *Appl. Environ. Microbiol* **2003**, *69*, 2245–2252. [CrossRef]
22. Zhu, K.; Frehan, S.K.; Mul, G.; Huijser, A. Dual role of surface hydroxyl groups in the photodynamics and performance of NiO-based photocathodes. *J. Am. Chem. Soc.* **2022**, *144*, 11010–11018. [CrossRef]
23. Jamali, R.; Bordbar-Khiabani, A.; Yrmand, B.; Mozafari, M.; Kolahi, A. Effects of co-incorporated ternary elements on biocor rosion stability, antibacterial efficacy, and cytotoxicity of plasma electrolytic oxidized titanium for implant dentistry. *Mater. Chem. Phys.* **2022**, *276*, 125436. [CrossRef]
24. Gebre, S.H.; Sendeku, M.G. New frontiers in the biosynthesis of metal oxide nanoparticles and their environmental applications: An overview. *SN Appl. Sci.* **2019**, *1*, 928. [CrossRef]
25. Nakayama, S.; Notoya, T.; Osakai, T. Highly selective determination of copper corrosion products by voltammetric reduction in a strongly alkaline electrode. *Anal. Sci.* **2012**, *28*, 323–331. [CrossRef] [PubMed]
26. Momose, Y.; Kohno, S.; Honma, M.; Kamosawa, T. Temperature programmed photoelectron emission analysis of copper sur faces subjected to cleaning and abrasion in organic liquids. In Proceedings of the 2nd International Conference in Processing Materials for Properties, San Francisco, CA, USA, 5–8 November 2000; TMS: Warrendale, PA, USA, 2000; pp. 285–290.
27. Momose, Y.; Honma, M.; Kamosawa, T. Temperature-programmed photoelectron emission technique for metal surface anal ysis. *Surf. Interface Anal.* **2000**, *30*, 364–367. [CrossRef]
28. Kamosawa, T.; Honma, M.; Momose, Y. Observation of real metal surfaces by temperature programmed photoelectron emis sion technique-temperature dependence of the amount of emitted electrons and its relationship to XPS analysis. *J. Surf. Finish. Soc. Jpn.* **2000**, *51*, 836–843. (In Japanese) [CrossRef]
29. Momose, Y.; Sato, K.; Ohno, O. Electrochemical reduction of CO_2 at copper electrodes and its relationship to the metal surface characteristics. *Surf. Interface Anal.* **2002**, *34*, 615–618. [CrossRef]
30. Wagner, C.D. *Handbook of X-ray Photoelectron Spectroscopy*; Perkin-Elmer: Eden Prairie, MN, USA, 1979.
31. Evans, S. Oxidation of the group IB metals studied by X-ray and ultraviolet photoelectron spectroscopy. *J. Chem Soc. Faraday Trans. II* **1975**, *71*, 1044–1057. [CrossRef]
32. McIntyre, N.S.; Sunder, S.; Shoesmith, D.W.; Stanchell, F.W. Chemical information from XPS-applications to the analysis of electrode surfaces. *J. Vac. Sci. Technol.* **1981**, *18*, 714–721. [CrossRef]
33. Morohashi, H.; Shibuya, K.; Amaki, Y. *Surface Analysis of Tarnished Copper Plate, Report of the Industrial Research Institute of Niigata Prefecture*; No. 50 2020; The Industrial Research Institute of Niigata Prefecture: Niigata, Japan, 2021; pp. 68–71.
34. Abe, Y.; Kusakabe, C.; Nakao, I.; Tanaka, Y.; Yamabe, S. Theoretical study on the 1:1 solvation of triethylphosphine oxide with the solvent molecule–Correlation between empirical solvent parameter AN based on 31P NMR chemical shift and MO calculations. *J. Comput. Aided Chem.* **2007**, *8*, 59–68. [CrossRef]
35. Huheey, J.E. *Inorganic Chemistry, Principles of Structure and Reactivity*, 3rd ed.; Harper & Row: New York, NY, USA, 1983; Japanese Translation by Kodama, G.; Nakazawa, H. Tokyo Kagaku Dojin (Tokyo, 1984); pp. 340–341.
36. Available online: http://www.stenutz.eu/chem/solv21.php (accessed on 5 January 2024).
37. Riddick, J.A.; Bunger, W.B. *Organic Solvents*, 3rd ed.; Wiley-Interscience: New York, NY, USA, 1970.
38. Ramsey, J.A. The adsorption of gases on clean metal surfaces and exoelectron emission. *Jpn. J. Appl. Phys.* **1985**, *24* (Suppl. 4), 32–37. [CrossRef]
39. Huheey, J.E. *Inorganic Chemistry, Principles of Structure and Reactivity*, 2nd ed.; Harper International Edition; Harper & Row: New York, NY, USA, 1978; p. 47.
40. Momose, Y.; Suzuki, D.; Tsuruya, K.; Sakurai, T.; Nakayama, K. Transfer of electrons on scratched iron surfaces: Photoelectron emission and X-ray photoelectron spectroscopy studies. *Friction* **2018**, *6*, 98–115. [CrossRef]
41. Kittel, C. *Introduction to Solid State Physics*, 2nd ed.; Uno, R.; Tsuya, N.; Morita, A.; Yamashita, J., Translators; John Wiley & Sons: New York, NY, USA, 1956; p. 300. (In Japanese)
42. Juse, W.P.; Kurtschatow, B.W. Electrical conductivity of Cu_2O. *Phys. Zeits. Sowjetunion* **1933**, *2*, 453.
43. Mott, N.F.; Gurney, R.W. *Electronic Processes in Ionic Crystals*, 2nd ed.; Clarendon: Oxford, UK, 1957; pp. 163–164.

Disclaimer/Publisher's Note: The statements, opinions and data contained in all publications are solely those of the individual author(s) and contributor(s) and not of MDPI and/or the editor(s). MDPI and/or the editor(s) disclaim responsibility for any injury to people or property resulting from any ideas, methods, instructions or products referred to in the content.